Phytophthora infestans effector SFI3 targets potato UBK to suppress early immune transcriptional responses

He, Qin; McLellan, Hazel; Hughes, Richard K.; Boevink, Petra C.; Armstrong, Miles; Lu, Yuan

Published in:
New Phytologist

DOI:
10.1111/nph.15635

Publication date:
2019

New Phytologist

Research

Phytophthora infestans effector SFI3 targets potato UBK to suppress early immune transcriptional responses

Qin He[1,2,3], Hazel McLellan[2], Richard K. Hughes[4], Petra C. Boevink[3], Miles Armstrong[2,3], Yuan Lu[1], Mark J. Banfield[4], Zhendong Tian[1] and Paul R. J. Birch[2,3]

[1]Key Laboratory of Horticultural Plant Biology (HZAU), Ministry of Education, Key Laboratory of Potato Biology and Biotechnology, Ministry of Agriculture, Huazhong Agricultural University, Wuhan, Hubei 430070, China; [2]Division of Plant Science, School of Life Science, University of Dundee (at JHI), Invergowrie, Dundee, DD2 5DA, UK; [3]Cell and Molecular Science, James Hutton Institute, Invergowrie, Dundee, DD2 5DA, UK; [4]Department of Biological Chemistry, John Innes Centre, Norwich Research Park, Norwich, NR4 7UH, UK

Authors for Correspondence:
Paul R. J. Birch
Tel: +44 1382 568830
Email: Paul.Birch@hutton.ac.uk

Zhendong Tian
Tel: +86 02787286939
Email: tianzhd@mail.hzau.edu.cn

Received: *22 June 2018*
Accepted: *19 November 2018*

New Phytologist (2019)
doi: 10.1111/nph.15635

Key words: disease resistance, effector-triggered susceptibility, pathogenicity, potato late blight, virulence.

Summary

- The potato blight agent *Phytophthora infestans* secretes a range of RXLR effectors to promote disease. Recent evidence indicates that some effectors suppress early pattern-triggered immunity (PTI) following perception of microbe-associated molecular patterns (MAMPs). *Phytophthora infestans* effector PiSFI3/Pi06087/PexRD16 has been previously shown to suppress MAMP-triggered *pFRK1-Luciferase* reporter gene activity. How PiSFI3 suppresses immunity is unknown.
- We employed yeast-two-hybrid (Y2H) assays, co-immunoprecipitation, transcriptional silencing by RNA interference and virus-induced gene silencing (VIGS), and X-ray crystallography for structure-guided mutagenesis, to investigate the function of PiSFI3 in targeting a plant U-box-kinase protein (StUBK) to suppress immunity.
- We discovered that PiSFI3 is active in the host nucleus and interacts in yeast and *in planta* with StUBK. UBK is a positive regulator of specific PTI pathways in both potato and *Nicotiana benthamiana*. Importantly, it contributes to early transcriptional responses that are suppressed by PiSFI3. PiSFI3 forms an unusual *trans*-homodimer. Mutation to disrupt dimerization prevents nucleolar localisation of PiSFI3 and attenuates both its interaction with StUBK and its ability to enhance *P. infestans* leaf colonisation.
- PiSFI3 is a 'WY-domain' RXLR effector that forms a novel *trans*-homodimer which is required for its ability to suppress PTI via interaction with the U-box-kinase protein StUBK.

Introduction

The plant immune system may be activated following the detection of conserved microbial molecules (microbe-associated molecular patterns, MAMPs) by cell surface pattern recognition receptors (PRRs). Pathogen effectors serve to suppress this pattern-triggered immunity (PTI), or otherwise manipulate processes in the host to promote susceptibility. Effectors may be delivered by microbial pathogens to act in the apoplast or within plant cells (Jones & Dangl, 2006).

The late blight pathogen *Phytophthora infestans* remains a constant threat to potato and tomato production, precipitating considerable crop losses annually (Fry *et al.*, 2015; Kamoun *et al.*, 2015). Amongst a large repertoire of virulence determinants are the RXLR effectors, so-called because of the conserved Arg−any amino acid−Leu−Arg motif that facilitates their delivery inside plant cells (Rehmany *et al.*, 2005; Whisson *et al.*, 2007; Wawra *et al.*, 2017). RXLR effectors manipulate a range of host processes by direct interaction with diverse plant proteins (Whisson *et al.*, 2016). Some host proteins targeted by *P. infestans* RXLR effectors are positive regulators of immunity that confer posttranslational modifications (PTMs). For example, the RXLR effector AVR3a targets CMPG1, a host ubiquitin E3 ligase required for cell death triggered by perception of the PAMP infestin-1 (INF1; Bos *et al.*, 2010) and a range of additional pathogen elicitors perceived at the cell surface (Gilroy *et al.*, 2011). RXLR effector PexRD2 targets the kinase domain of the host protein MAP3Kε, which mediates signal transduction following perception of *Cladosporium fulvum* apoplastic effector Avr4 by the tomato Cf4 resistance protein (King *et al.*, 2014).

By contrast to these examples, *P. infestans* RXLR effectors also target host proteins conferring PTMs that act as negative regulators of immunity, the so-called susceptibility (S) factors (Boevink *et al.*, 2016a). For example, effector Pi02860 suppresses INF1-mediated cell death and interacts with host protein StNRL1, which is predicted to complex with Cullin 3 to act as an E3 ligase (Yang *et al.*, 2016). However, StNRL1 is a negative regulator of INF1-mediated cell death, and therefore Pi02860 promotes its activity in targeting the positive immune regulator SWAP70 for proteasome-mediated degradation (He *et al.*, 2018). In addition,

whereas PexRD2 suppresses the kinase signalling activity of its target MAP3Kε (King *et al.*, 2014) to prevent phosphorylation of its substrates, RXLR effector Pi04314 interacts with protein phosphatase 1 (PP1) catalytic isoforms to form holoenzymes that are predicted to dephosphorylate substrates (Boevink *et al.*, 2016b), and effector Pi17316 targets the MAP3K VIK to support its activity as a negative regulator of immunity (Murphy *et al.*, 2018). These examples demonstrate that oomycetes can alter PTMs that positively or negatively regulate immunity.

Phosphorylation and ubiquitination are pervasive PTMs that affect all processes inside eukaryotic cells. The interplay and cross-talk between the two events have become a recurrent theme in cell signalling regulation (Nguyen *et al.*, 2013; Filipčík *et al.*, 2017). Protein kinases and ubiquitin E3 ligases play roles in both positive and negative regulation of PTI and ETI. Many PRRs involved in pathogen detection, for example, are kinases that initiate phosphorylation cascades (e.g. Wang *et al.*, 2018). PRRs activate mitogen-activated protein kinase (MAPK) cascades involved in regulating immunity (Mithoe & Menke, 2018). In addition, kinases activate transcriptional regulators of immunity (Ishihama & Yoshioka, 2012), and regulate the complex cross-talk between phytohormone signalling pathways (Chen *et al.*, 2010b). On the ubiquitination side, in addition to CMPG1 and NRL1, another E3 ubiquitin ligase, PUB17, functions in the host nucleus to mediate both PTI, following perception of the bacterial PAMP flg22, and cell death triggered by expression of Cf4/Avr4 but not INF1 (He *et al.*, 2015). By contrast with CMPG1 and PUB17, some PUB E3 ligases have been shown to negatively regulate immunity. Two U-box E3 ligases, PUB12 and PUB13, negatively regulate flagellin (flg22)-triggered defense responses via the ubiquitination-mediated turnover of FLS2 (Lu *et al.*, 2011; Kong *et al.*, 2015). PUB22 targets a subunit of the exocyst complex, Exo70B2 for proteasomal degradation required for PAMP-triggered responses in Arabidopsis (Stegmann *et al.*, 2012). More recently, the substrate adaptor component of a CULLIN3-based E3 ligase, POB1, has been show to negatively regulate a range of immune responses and, indeed, one of its substrates for proteasome-mediated degradation is PUB17 (Orosa *et al.*, 2017).

In this study, we focused on an RXLR effector from *P. infestans*, SFI3/Pi06087/PexRD16, which is upregulated during the biotrophic phase of leaf and tuber infection in strains from diverse geographical locations (Haas *et al.*, 2009; Oh *et al.*, 2009; Cooke *et al.*, 2012; Ah-Fong *et al.*, 2017; Yin *et al.*, 2017). Unlike PiSFI5, which suppresses flg22-triggered immunity upstream of MAP kinases activation by interacting with calmodulin (Zheng *et al.*, 2018), PiSFI3 was able to suppress flg22-induced *promoter-FLG22-INDUCED RECEPTOR-LIKE KINASE1 – LUCIFERASE (pFRK1-Luc)* reporter gene activity downstream of MAP kinase activation in protoplasts of the host plant tomato (Zheng *et al.*, 2014). Here, we show that when expressed in *N. benthamiana* or potato, PiSFI3 acts in the nucleus to enhance *P. infestans* leaf colonization. Overexpression of PiSFI3 in transgenic potato lines suppressed early transcriptional responses triggered by flg22. PiSFI3 interacts with a protein containing both U-box and kinase domains, StUBK, in yeast-two-hybrid (Y2H) assays and *in planta*. Silencing of *UBK* in *N. benthamiana* by virus-induced gene silencing (VIGS) or in potato by RNAi enhanced *P. infestans* leaf colonization. Transient expression of StUBK reduces *P. infestans* colonization and prevents PiSFI3 virulence activity. Moreover, VIGS or RNAi of *UBK* suppresses early transcriptional responses triggered by flg22 but has no effect on the cell death triggered by *P. infestans* PAMP INF1 and Cf4/Avr4 co-expression. The crystal structure of PiSFI3 confirms it possesses the WY-domain fold (Boutemy *et al.*, 2011), but adopts an unusual *trans*-homodimer and can oligomerise *in planta*. Mutation of pairs of Leu/Asp residues that face each other across the PiSFI3 α-helices, disrupted oligomerisation, and attenuated virulence function. We further found that PiSFI3 Leu/Asp mutants failed to localize in the nucleolus and were not able to interact with StUBK, demonstrating that interaction with StUBK is required for the virulence function of PiSFI3.

Materials and Methods

Plasmid constructs

The full-length *StUBK* gene was cloned from potato cDNA with gene-specific primers modified to contain the Gateway® (Invitrogen) attB recombination sites. Polymerase chain reaction (PCR) products were purified and recombined into pDONR201 (Invitrogen) to generate entry clones. SFI3, minus the signal peptide-encoding portion, was amplified from *P. infestans* cDNA and cloned into pDONR201. Primer sequences are shown in Supporting Information Table S1. Protein fusions were made by recombining the entry clones with the following plant expression vectors: pB7WGF2, pK7WGR2 and pGWB18 to generate N-terminal green fluorescent protein (GFP), monomeric red fluorescent protein (mRFP) and cMyc fusions respectively. SFI3 double mutant clones were obtained by gene synthesis (Genesys, Genscript HK Ltd, Hong Kong, China) and cloned as above.

Potato transformation and plant growth condition

The RNAi construct was designed in the nonconserved 5′ regions of *NbUBK* and cloned into the expression vector pHellsgate 8. Primer sequences are shown in Table S1. *Agrobacterium tumefaciens* containing the RNAi vector was transformed into the potato cultivar E3 by microtuber disc transformation as described by Si *et al.* (2003). Putative transgenic potato plants harbouring the target gene construct were screened on differential medium (3% Murashig and Skoog medium (MS) + 0.2 mg l^{-1} indole-3-acetic acid + 0.2 mg l^{-1} gibberellin A3 + 0.5 mg l^{-1} 6-Benzyl aminopurine + 2 mg l^{-1} zeatin + 75 mg l^{-1} kanamycin (kan) + 200 mg l^{-1} cephalosporins (Cef), pH 5.9) and then transferred to root generation medium (3% MS + 50 mg l^{-1} kan + 400 Cef mg l^{-1}, pH 5.9). Transformants were confirmed by PCR with a forward primer binding to the 35S promotor and a gene-specific reverse primer. Gene expression levels were analyzed by qRT-PCR. The potato plantlets were propagated in MS medium (4% sucrose and 0.7% agar) and raised in a climate-controlled room at 20°C (16 h : 8 h, light : dark cycle).

Phytophthora infestans infection assay

Phytophthora infestans 88069tdT10 was grown in Petri dishes (90 mm diameter) of rye agar medium supplemented with geneticin antibiotic at 19°C. The *P. infestans* strain, Ljx18 (race 3.4.7.10.11) and HB09-14-2 (race 1.2.3.4.5.6.7.9.10.11, collected from Hubei Province, China), were cultured and propagated on rye agar at 19°C. Spores were prepared from cultures grown for 13 d. The spore concentration for the inoculum was adjusted by dilution in sterile distilled water to yield 4×10^4 sporangia ml^{-1} for *N. benthamiana* leaves (VIGS leaves and transient expression assays), higher inoculum (8×10^4) sporangia ml^{-1} for GFP–StUBK transient expression assays and infection, and 7×10^4 sporangia ml^{-1} for potato leaves. Next, 10 µl droplets were inoculated onto the abaxial side of detached *N. benthamiana* (four sites per leaf) or potato leaves (two sites per leaf). Inoculated leaves were stored on moist tissue in sealed boxes. The infection assays were carried out as described previously (He *et al.*, 2015; Boevink *et al.*, 2016b; Yang *et al.*, 2016).

Tobacco rattle virus (TRV)-based VIGS in *N. benthamiana*

Two portions of the nonconserved 5′ region of *NbUBK* were selected to make VIGS constructs. Regions were selected that shared no significant homology with other sequences in *N. benthamiana* to minimise the potential for off-target silencing. The two regions of *NbUBK* were amplified from *N. benthamiana* cDNA and cloned into pBinary TRV vectors (Liu *et al.*, 2002) between *Hpa*I and *Eco*RI restriction enzyme recognition sites in the antisense orientation. A TRV construct expressing GFP was used as a control (Gilroy *et al.*, 2007). The VIGS agroinfiltration was carried out as described previously (He *et al.*, 2015; Boevink *et al.*, 2016b; Yang *et al.*, 2016). The silencing level of *NbUBK* was analysed by qRT-PCR 2–3 wk after infiltration. Silenced-leaves 3 wk after infiltration were used for *P. infestans* colonization, HR assays or flg22 treatment. For each assay, six independent plants were used for each VIGS construct, with three biological replicates.

Heterologous expression in *E. coli*, protein production and purification

SFI3 lacking the first 48 N-terminal amino acids (signal peptide and RXLR sequences removed), was cloned into the pOPINF plasmid (Berrow *et al.*, 2007) by In-Fusion cloning (Clontech) following PCR using forward (AAGTTCTGTTTCAGGG CCCGTCGATTGCGGCAATTCTCGCCGAAGCGGG) and reverse (ATGGTCTAGAAAGCTTTAAGGTGTGGCCAG CCTCTTCTTCTCTTCTTTC) primers (Integrated DNA Technologies).

SFI3 protein was produced in *E. coli* BL21 (DE3) cells grown in Luria-Bertani medium until optical density (OD) reached $OD_{600\ nm}$ 0.5–0.8. Cultures were induced with 1 mM isopropyl-1-thio-β-D-galactopyranoside and incubated at 18°C for 18 h. Cell pellets were frozen at −80°C overnight and resuspended in 50 mM Tris−HCl buffer, pH 8.0 containing 0.5 M NaCl, 50 mM glycine, 5% (v/v) glycerol, 20 mM imidazole and protease inhibitors (complete EDTA-free tablets, one tablet per 50 ml, Roche). Cells were lysed by sonication. Histidine-tagged SFI3 was purified from cleared lysate using an ÄKTAxpress system (GE Healthcare) by IMAC on a 5 ml Ni^{2+} His-Trap FF column followed by gel filtration on a Superdex 75 26/60 column pre-equilibrated in 20 mM HEPES, pH 7.5 containing 0.15 M NaCl (gel filtration buffer). Eluted monomeric protein was cleaved overnight at 4°C with histidine-tagged 3C protease (10 µg/mg protein) in gel filtration buffer supplemented with 5 mM β-mercaptoethanol. Cleaved SFI3 protein was separated from uncleaved protein by IMAC chromatography, concentrated to 5–7 ml and re-purified by gel filtration as above. Monomeric protein was concentrated to 16 mg ml^{-1}, frozen in 50 µl aliquots in liquid nitrogen and stored at −80°C. SFI3 protein concentration was estimated by measuring absorbance at 280 nm and predicted extinction coefficients for the fusion and cleaved proteins of 19 940 M^{-1} cm^{-1}.

Crystallisation, data collection and structure solution

For crystallisation, SFI3 was concentrated to 20 mg ml^{-1}. Crystallisation experiments used 96-well plates, commercially available reagents, and were set up with an Oryx Nano robot (Douglas Instruments). Optimizations were carried out in 48-well plates, also using an Oryx Nano robot. For X-ray data collection, crystals were grown in 0.1 M bis-tris-propane pH 7.5, 0.2 M sodium acetate and 20% (w/v) polyethylene glycol (PEG) 3350, transferred to a cryoprotectant solution containing 0.1M bis-tris-propane pH 7.5, 0.2 M sodium acetate and 35% (w/v) PEG 3350, mounted in a litho-loop and flash cooled in liquid nitrogen. To enable collection of anomalous X-ray data for structure solution, crystals were soaked for *c.* 60 s in a well solution supplemented with 0.1 M potassium iodide and cryoprotected as above before flash freezing in liquid nitrogen.

Native and single wavelength anomalous diffraction (SAD) X-ray data sets were collected at the Diamond Light Source, United Kingdom, beamline I02 (under beamtime allocation MX1219). The data were processed using xia2 (Winter, 2010), and scaled with SCALA from the CCP4 suite (Winn *et al.*, 2011). The structure was solved using SAD data collected from a crystal soaked in potassium iodide solution. Lodide sites were identified with Phenix, which was also used to calculate phases and generate initial electron density maps. The experimental phases were then used by ARP/wARP, as implemented in CCP4, to autobuild the first model. This model was subsequently used to phase a second crystal form by molecular replacement. The final model (in the latter crystal form) was produced through iterative rounds of refinement using REFMAC5 (Murshudov *et al.*, 1997) and manual rebuilding with COOT (Emsley *et al.*, 2010). Structure validation used the tools provided in COOT and MOLPROBITY (Chen *et al.*, 2010a,b).

The co-ordinates and structure factors for SFI3 have been deposited at the Protein Data Bank (PDB) with accession number 6GU1.

Agrobacterium-mediated transient expression

Agrobacterium-mediated transient expression by agroinfiltration was performed as described previously (Gilroy *et al.*, 2011; Yang *et al.*, 2016; Boevink *et al.*, 2016b). *Agrobacterium* strains were infiltrated into leaves of *N. benthamiana* wild-type or VIGS plants. The concentrations measured by absorbance at 600 nm of *A. tumefaciens* used were: 0.1–0.01 for confocal imaging, 0.5 for western blot analyses and HR assays and 0.1 for agroinfiltration and infection assays. For co-expression of multiple constructs *A. tumefaciens* suspensions of strains carrying the different constructs were thoroughly mixed before infiltration.

Confocal microscopy

Agrobacterium tumefaciens containing target protein fusions were infiltrated into leaves of 4-wk-old *N. benthamiana* plants. *Nicotiana benthamiana* leaf cells expressing fluorescent protein fusions were imaged no later than 2 d after agroinfiltration using a Nikon A1R confocal microscopes confocal microscope. GFP was excited with 488 nm from an argon laser and its emissions were detected between 500 and 530 nm. Images were collected from leaf cells expressing low levels of the protein fusions to minimise artefacts of ectopic protein expression. MG132 (40 μM) was infiltrated into leaves 6 h before imaging under the confocal microscope.

Yeast-two-hybrid

A Y2H screen with pDEST32-PiSFI3 was performed as described in McLellan *et al.* (2013) using the Invitrogen ProQuest system. The full-length coding sequence of the candidate interacting prey sequence (U-box kinase) was cloned and re-tested with pDEST32-PiSFI3 and use pDEST32-Pi04089 as a control to rule out the possibility that the observed reporter gene activation had resulted from interactions between the prey and the DNA-binding domain of the bait construct or DNA-binding activity of the prey itself. For each transformation, 1 μg plasmid DNA and 100 μg denatured sheared salmon sperm DNA were mixed together with 100 μl of the yeast suspension; 700 μl of 1× lithium acetate/40% PEG 3350/1× Tris−EDTA (TE) buffer were added, mixed well and incubated at 30°C for 30 min; 88 μl dimethyl sulphoxide (DMSO) were added, mixed well, heat shocked at 42°C for 7 min, centrifuged for 10 s and the supernatant was removed. The pellet was resuspended in 1 ml 1× TE and re-pelleted; the pellet was resuspended in 50-100 μl TE and plated on a selective media. Transformants were identified by testing reporter gene activation in the X-gal assay.

Co-immunoprecipitation analyses

The fused protein constructs were transiently overexpressed in *N. benthamiana* by *Agrobacterium*-mediated expression. Leaf samples were collected 48 h after infiltration. Proteins were extracted by using GTEN buffer (25 mM Tris−HCl pH 7.5, 1 mM EDTA,150 mM NaCl,10% glycerol) with 10 mM dithiothreitol (DTT), protease inhibitor cocktail (PIC), 1 mM pregnant mare's serum gonadotropin (PMSF) and 0.2% Nonidet P40. Samples were ground in liquid nitrogen with 500 μl extraction buffer on ice, gently vortexed and placed on ice and centrifuged at 13 000 ***g*** for 10 min at 4°C; the supernatant was transferred to a precooled tube (re-spun if leaf tissues were present in the supernatant, until clear); To 50 μl sample (input) 50 μl 2× sample buffer were added and boiled at 95°C for 10 min and stored at −20°C for western blot analysis; 450 μl of extract was kept for the co-immunoprecipitation (Co-IP); 20–25 μl beads were used per immunoprecipitation (IP). The required amount was taken and washed three times with ice-cold dilution/wash buffer; washed beads were added to cell lysates and shaken for 1–2 h at 4°C or room temperature (RT). Beads were washed twice with 500 μl ice cold wash buffer, resuspended in 50 μl 2× sodium dodecyl sulphate (SDS) buffer and boiled at 95°C for 10 min. The samples were stored at −20°C for western analysis. mRFP-tagged or GFP-tagged fusions were immunoprecipitated using mRFP–Trap®-M magnetic beads or GFP–Trap®-M magnetic beads (Chromotek Gmbh), respectively. The resulting samples were separated by SDS-PAGE and western blotting. Immunoprecipitated RFP fusions and co-immunoprecipitated c-*MYC* fusions were detected using appropriate antisera.

Flg22 treatment and gene expression assays

Here, 6-wk-old potato plants or 3-wk-old VIGS plants were used for the treatments. Three leaves from the third to the fifth compound leaf from the top of each potato lines or three leaves from VIGS-plants were infiltrated with flg22 (40 mM). Three leaves per time point each were harvested from separate plants and snap frozen in liquid nitrogen. The RNA was extracted and cDNA was made and diluted to 1 : 20 for RT-PCR using the marker genes. Primer pairs were designed outside the region of cDNA targeted for silencing following the manufacturer's guidelines. Primer sequences are given in Table S1. Relative expression of the target genes was calculated using the 2ΔΔCt method with *StTubulin* as the reference for potato, *NbEf1a* for *N. benthamiana*. *Actin* was used as the reference of potato for semi-quantified RT-PCR.

The *P. infestans* biomass was quantified by qPCR using *Ef-1a* (used to quantify *S. tuberosum* DNA) and PiO8 primers (designed based on highly repetitive sequences from the *P. infestans* genome to quantify *P. infestans* DNA) as described by Llorente *et al.* (2010). Three leaves for each time point (every 24 h after inoculation with *P. infestans*) were harvested and snap frozen in liquid nitrogen. The DNA was extracted and quantified by qRT-PCR.

Results

Nuclear localization of GFP–PiSFI3 is important for *P. infestans* virulence

Transient expression of GFP–PiSFI3 in *N. benthamiana* showed that it was enriched in the nucleus/nucleolus and enhanced

colonization by *P. infestans* (Zheng *et al.*, 2014). To investigate whether the nucleus is an important site of PiSFI3 activity within host cells, we misdirected its localization. In addition to GFP–PiSFI3, two fusion constructs were generated, either with a nuclear export signal (NES; $_{NES}$GFP–PiSFI3) or with a nuclear localization signal (NLS; $_{NLS}$GFP–PiSFI3), as described for other RXLR effectors (Boevink *et al.*, 2016b; Yang *et al.*, 2016). As shown previously (Zheng *et al.*, 2014, 2018), GFP–PiSFI3 accumulated strongly in the nucleus, forming a ring around the nucleolus, with additional cytoplasmic background (Fig. 1a). By contrast, $_{NES}$GFP–PiSFI3 fluorescence was observed primarily in the cytoplasm, whereas $_{NLS}$GFP–PiSFI3 fluorescence was focussed in the nucleus and nucleolus (Fig. 1a). GFP–PiSFI3, $_{NLS}$GFP–PiSFI3 and $_{NES}$GFP–PiSFI3 fusions were expressed transiently in *N. benthamiana* and the leaves were challenged with *P. infestans* 1 d after agroinfiltration. Lesion size was recorded after 6 d. As described in Zheng *et al.* (2014, 2018), GFP–PiSFI3 enhanced colonization by *P. infestans*. Expression of $_{NLS}$GFP–PiSFI3 was found to also significantly promote larger *P. infestans* lesions compared with free GFP control (analysis of variance [ANOVA], $P < 0.001$). Lesion sizes following the expression of $_{NES}$GFP–PiSFI3 were reduced significantly compared with GFP–PiSFI3 and $_{NLS}$GFP–PiSFI3, but showed no significant difference compared to the empty GFP control (Fig. 1b, Supporting Information Figure S1). All constructs produced intact fusion proteins when expressed *in planta* (Fig. 1c). We therefore conclude that exclusion of PiSFI3 from the nucleus attenuates its contribution to virulence.

PiSFI3 attenuates early flg22-triggered transcriptional responses in potato

To determine whether PiSFI3 enhanced *P. infestans* colonization in potato, cultivar E-potato-3 (E3) was transformed with a construct expressing *35S:PiSFI3*. Six independent transgenic lines were selected for the preliminary experiments. Following inoculation of zoospores, pathogen colonisation was considerably enhanced ($P < 0.001$, one-way ANOVA) on the transgenic lines compared with the E3 control, as measured by lesion diameter at 5 d post-inoculation (dpi; Fig. S2). The transgenic lines expressing *SFI3* showed no developmental phenotype, and were similar to the E3 control. Two transgenic lines, PiSFI3-25 and

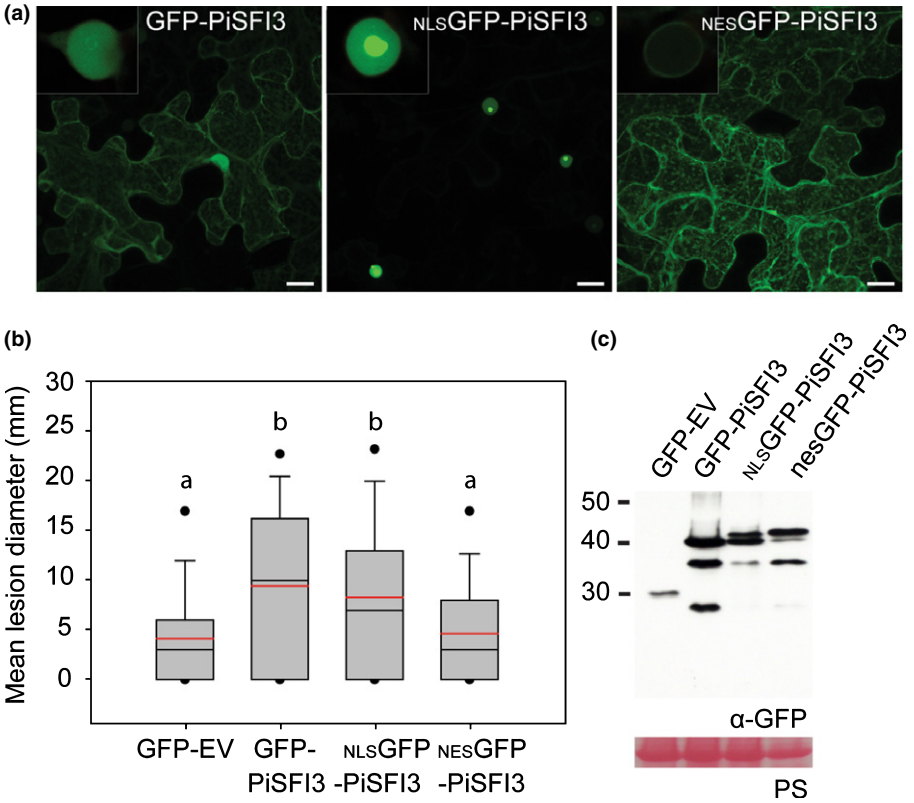

Fig. 1 Nuclear localization of GFP−PiSFI3 is important for *Phytophthora infestans* virulence. (a) Images are projections of confocal Z series showing that GFP-PiSFI3 is enriched in the nucleus/nucleolus with cytoplasmic background, while $_{NES}$GFP−PiSFI3 is greatly reduced in nuclear fluorescence, and $_{NLS}$GFP−PiSFI3 is concentrated in the nucleus/nucleolus and reduced in the cytoplasm. Bars, 10 mM. (b) GFP−PiSFI3 and $_{NLS}$GFP−PiSFI3 promote *P. infestans* growth following *Agrobacterium*-mediated expression compared to a GFP control. The $_{NES}$GFP−PiSFI3 does not significantly promote *P. infestans* infection compared to the control. Boxplots represent the combined data from three biological reps ($n = 56$). Letters above the boxplots denote statistically significant differences (ANOVA, $P < 0.001$). The red lines in the boxes represents the mean. The black lines represents the median. The black dot above and below each box represent the 95th and 5th percentage of outliers. (c) Western blotting indicates that the GFP−PiSFI3, $_{NLS}$GFP−PiSFI3 and $_{NES}$GFP−PiSFI3 fusions are stable *in planta* showing the expected protein size. Protein loading is indicated by Ponceau stain and the antibody used is αGFP. Protein size markers are indicated in kDa.

PiSFI3-26, were selected for further studies (Fig. 2a). These two lines showed significantly enhanced *P. infestans* colonization ($P < 0.001$, one-way ANOVA) compared with the E3 control, as measured by lesion diameter and sporangia number (Figs 2b–d, S2c). Moreover, *P. infestans* biomass, determined by qPCR measurement of pathogen DNA, was observed to increase more rapidly on the transgenic PiSFI3-25 and PiSFI3-26 lines between 2 and 3 dpi, which is the biotrophic phase of infection before symptom development (Fig. 2e). These results confirmed previous observations that transient expression of SFI3 on the model *P. infestans* host *Nicotiana benthamiana* also enhanced pathogen colonisation (Zheng *et al.*, 2014, 2018).

PiSFI3 was previously shown to act downstream of MAP kinase activation in suppressing *pFRK:luc* reporter gene induction following flg22 treatment (Zheng *et al.*, 2014). To determine whether PiSFI3 suppresses early flg22-mediated transcriptional responses on potato, two flg22 marker genes, *NbWRKY7* and *NbACRE31*, used previously in *N. benthamiana* (McLellan *et al.*, 2013), were selected and their expression in potato E3 assessed after flg22 treatment. Transcript accumulation of each gene was shown to peak as early as 30 min posttreatment with flg22 (Fig. S3), and this time point was therefore selected to study the transgenic lines. Following treatment of the transgenic lines and E3 control with flg22 peptide, transcript accumulation of both St*WRKY7* and St*ACRE31* (Figs 2f,g, S3c,d) was attenuated in the transgenic PiSFI3 lines compared to the E3 control, demonstrating that the effector also attenuates early flg22-mediated transcriptional responses in potato leaves.

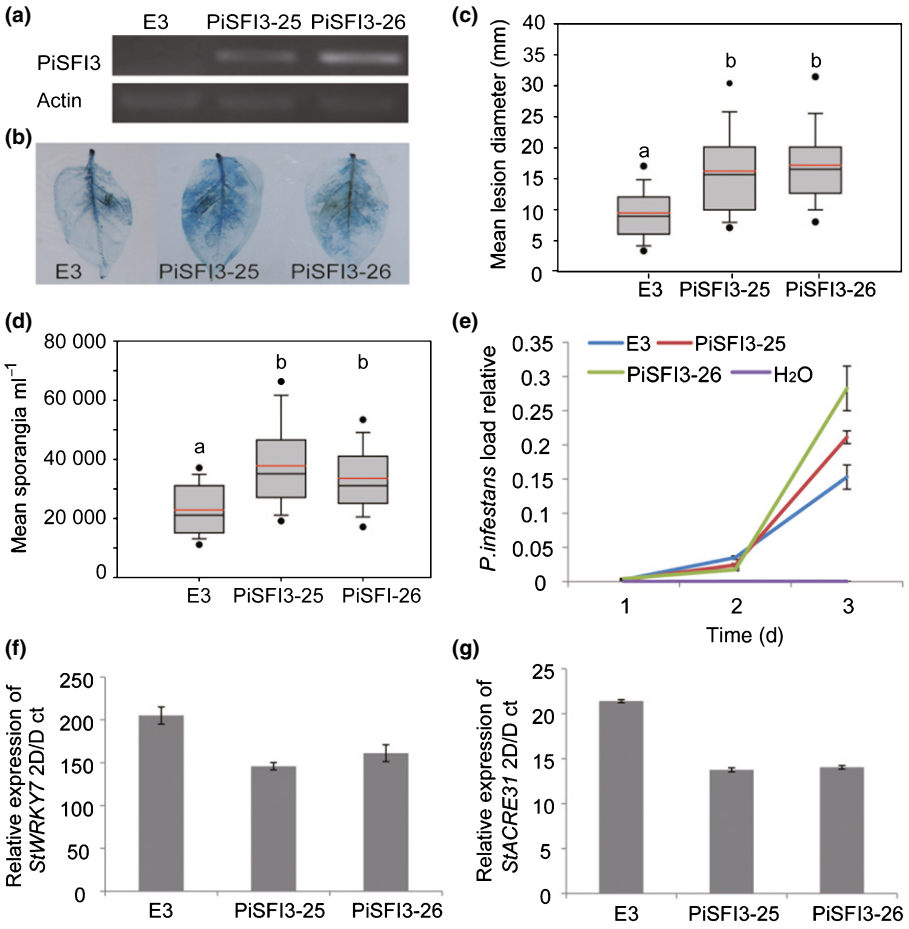

Fig. 2 PiSFI3 attenuates early flg22-triggered transcriptional responses in potato. (a) Gel images of a semi-quantitative PCR to compare *PiSFI3* and control *Actin* transcripts amplified from cDNA made from control and transgenic potato cultivar E3 (cv). (b) Representative trypan blue-stained leaf images of leaves of transgenic potatoes cv E3 expressing PiSFI3 and E3 controls infected with a mixture of two *Phytophthora infestans* isolates (HB09-14-2 and HB-0916-2) and photographed at 5 d post inoculation (dpi). (c) Boxplots shows the mean (red line) and median (black line) *P. infestans* lesion diameter of cultivar E3 and transgenic PiSFI3-expressing potato plants measured at 5 dpi. Boxplots represent the combined data from three biological reps (46 leaves per line). Letters on the boxplots denote statistically significant differences (ANOVA, $P < 0.001$). The black dots above and below each box represent the 95th and 5th percentage of outliers, respectively. (d) Overexpressing PiSFI3 allow a significant increase in *P. infestans* sporulation compared to the E3 control. Boxplots represent the combined data from three biological reps ($n = 120$). Letters on the boxplots denote statistically significant differences (ANOVA, $P < 0.001$). The black line represents the median line and the red line is the mean. The black dot above and below each box represent the 95th and 5th percentage of outliers. (e) Graph shows *P. infestans* biomass, determined by qPCR measurement of pathogen DNA using Ef-1α (used to quantify *Solanum tuberosum* DNA) and PiO8 primers (designed based on highly repetitive sequences from the *P. infestans* genome to quantify *P. infestans*. Three leaves for each time point (every 24 h after inoculation with *P. infestans*) were harvested and snap frozen in liquid nitrogen. The DNA was extract and quantified by qRT-PCR. Error bars show ± SE. (f, g) Relative expression of flg22 marker genes *StWRKY7* and *StACRE31* 30 min after treatment with flg22 in cv E3, PiSFI3-25 and PiSFI3-26 lines. Error bars show ± SE.

PiSFI3 does not suppress programmed cell death (PCD) triggered by INF1 or CF4/Avr4

In the previous study by Zheng *et al.* (2014, 2018), the three effectors that suppress flg22-mediated posttranslational MAP kinase activation (PiSFI5, PiSFI6, PiSFI7) were tested to see if they suppress two independent signal transduction pathways, triggered by expression of the elicitin infestin-1 (INF1), or by co-expression of tomato Cf4 with *Cladosporium fulvum* Avr4, which led to PCD. Whereas AVR3a was able to strongly suppress both INF1- and Cf4/Avr4-mediated PCD, only weak suppression was observed with PiSFI7, and only of INF1-mediated PCD (Zheng *et al.*, 2014, 2018). We therefore extended the analysis to PiSFI3. Again, whereas both INF1- and Cf4/Avr4-mediated PCD were strongly suppressed by the positive control, AVR3a, no such suppression was observed with PiSFI3 (Fig. S4). This result indicates that PTI suppression by PiSFI3 is restricted, in that it functions to attenuate flg22-mediated early transcriptional events but does not attenuate INF1-mediated PCD or, indeed, another pathway leading to PCD, triggered by Cf4 activation.

PiSFI3 interacts with a potato protein containing U-box and kinase domains

To investigate what PiSFI3 targets in the host to suppress flg22-mediated responses, a yeast-2-hybrid (Y2H) library of cDNA made from potato infected with *P. infestans* (Bos *et al.*, 2010) was screened with a GAL4 DNA binding domain-PiSFI3 fusion ('bait') construct to a depth of 2.6×10^6 yeast co-transformants. Twelve independent yeast colonies recovered from selection plates that contained GAL4 activation domain ('prey') fusions yielded sequences encoding a potato protein containing both U-box and kinase domains. The gene was therefore called *Solanum tuberosum U-box and kinase domain* (*StUBK*), and is a reciprocal best BLAST hit (candidate orthologue) of the gene *AtPUB33* in *Arabidopsis thaliana* (Fig. S5), the function of which is unknown. The plant U-box (PUB) domain is an ubiquitin E3 ligase domain and is uniquely combined with a kinase domain in AtPUB33. To confirm the Y2H interaction, a full-length *StUBK* sequence was cloned into the prey construct and tested pairwise with bait constructs containing PiSFI3, along with a control RXLR effector (Pi04089) which shares a similar nuclear and nucleolar localisation in plant cells, and which targets the RNA binding protein StKRBP1 (Wang *et al.*, 2015) and an empty bait vector (EV). Whereas all transformants grew on the control plates (+HIS) only yeast cells containing both PiSFI3 and StUBK were able to grow on the selection (−HIS) plates and activate the β-galactosidase (β-GAL) reporter (Fig. 3a).

To confirm that PiSFI3 and StUBK also interact *in planta*, co-immunoprecipitation (Co-IP) experiments were performed using cMYC–PiSFI3 and N-terminal mRFP-tagged StUBK (mRFP–StUBK), with cMYC–GUS and mRFP–GUS used as controls. The mRFP and cMYC fusion constructs were transiently co-

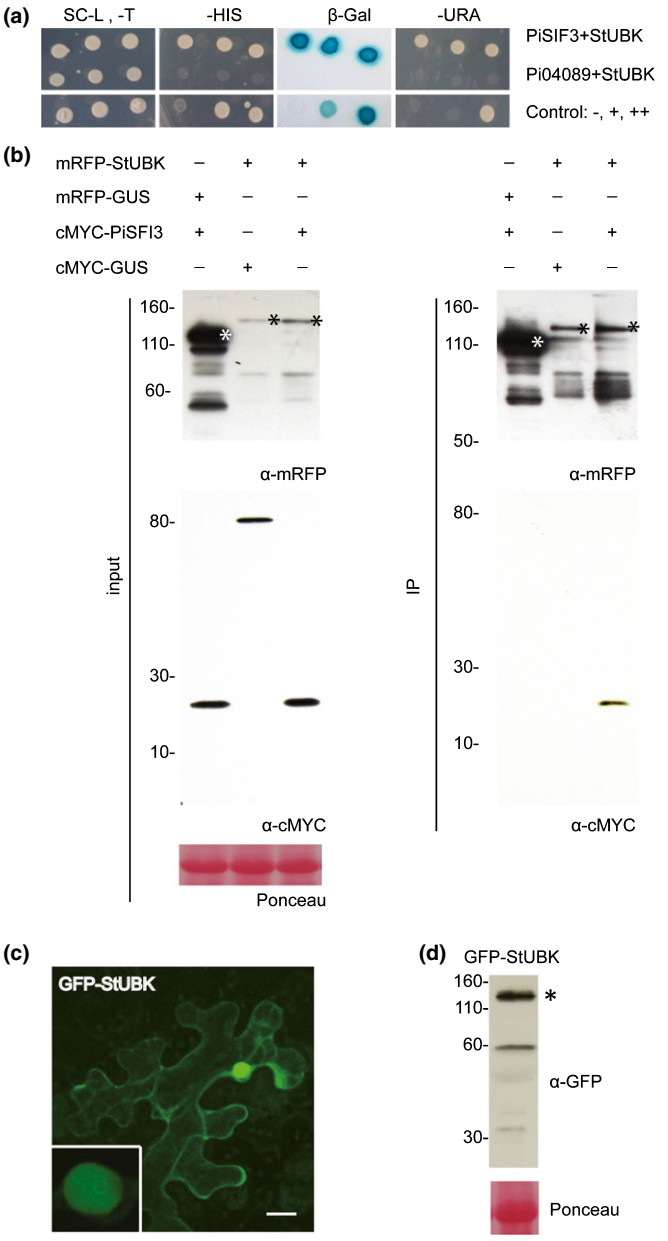

Fig. 3 PiSFI3 interacts with a potato protein containing U-box and kinase domains. (a) Yeast co-expressing StUBK with PiSFI3 grew on −histidine (−HIS) medium and yielded β-galactosidase (β-Gal) activity, while those co-expressed with the control Pi04089 did not. The +HIS control shows all yeast were able to grow in the presence of histidine.
(b) Immunoprecipitation (IP) of protein extracts from agroinfiltrated leaves using mRFP−Trap confirmed that mRFP-tagged StUBK specifically associated with cMYC−SFI3 and not with the cMYC−GUS control. cMYC−SFI3 specifically associated with mRFP−StUBK and not with the mRFP−GUS control. Expression of constructs in the leaves is indicated by '+'. Protein size markers are indicated in kDa, and protein loading is indicated by Ponceau stain. Stars show the mRFP-tagged fusion proteins for each construct. (c) Confocal images showing that GFP−StUBK is localised in the nucleus/nucleolus with cytoplasmic background. Bar, 10 mM. (d) Western blot indicates that GFP−StUBK is a stable fusion protein (star) *in planta*. Protein loading is indicated by Ponceau stain and the antibody used is αGFP. Protein size markers are indicated in kDa. The star shows the fusion protein of GFP–StUBK.

expressed in *N. benthamiana*. While all constructs were detected in the relevant input fractions, only cMYC–PiSFI3 and not the cMYC–GUS control was co-immunoprecipitated on mRFP–TRAP_M beads in the presence of mRFP–StUBK, and mRFP–GUS was unable to co-immunoprecipitate cMYC–PiSFI3 (Fig. 3b). As an additional control, we demonstrated that, by contrast to PiSFI3, the nuclear effector control Pi04089 failed to interact with mRFP–StUBK *in planta* (Fig. S6a).

To investigate the subcellular localization of StUBK, GFP was fused to its N terminus to form GFP–StUBK and viewed following *Agrobacterium*-mediated expression in *N. benthamiana* using confocal microscopy. GFP–StUBK protein localized in the nucleus with a ring around the nucleolus, and showed additional cytoplasmic fluorescence background (Fig. 3c), which is a similar localization to PiSFI3 (Fig. 3c). GFP–StUBK was stable as a fusion protein *in planta* (Fig. 3d).

Silencing of *UBK* enhances *P. infestans* leaf colonisation

To investigate a possible contribution of UBK to immunity, VIGS was used to knock-down *NbUBK* transcript levels in *N. benthamiana. Nicotiana benthamiana* is an alternative host for *P. infestans* and serves as a model for studying late blight, as it allows transient *Agrobacterium*-mediated gene expression, VIGS and noninvasive confocal microscopy to aid functional studies of molecular interactions between host and pathogen (e.g. Bos *et al.*, 2010; McLellan *et al.*, 2013; King *et al.*, 2014; Zheng *et al.*, 2014, 2018; Boevink *et al.*, 2016b; Murphy *et al.*, 2018).

Two independent TRV constructs (UBK-V1 and UBK-V2) were generated to specifically silence *NbUBK* by cloning two portions of the gene upstream of the conserved U-box and kinase domains to avoid off-target silencing (Fig. S7a). qRT-PCR was used to test silencing levels in each of three independent biological replicates and showed that transcript levels of *NbUBK* were reduced by 60–90% (Fig. S7b). *Nicotiana benthamiana* plants expressing UBK-V1 or UBK-V2 constructs consistently showed increased *P. infestans* colonisation compared to control TRV-GFP plants, measured as the percentage of inoculation sites that developed lesions ($P < 0.001$, one-way ANOVA) and by counting the numbers of sporangia developing on leaves at 8 dpi ($P < 0.002$, one-way ANOVA; Fig. 4a–c). This indicates that silencing *NbUBK* leads to increased susceptibility.

To investigate whether silencing *StUBK* has a similar effect on pathogenesis in potato, an antisense construct was generated, using the equivalent portion of the *StUBK* gene that was cloned from *NbUBK* in order to generate TRV construct UBK-V2 (Fig. S7c). This construct was transformed into potato cv E3. Six RNAi lines generated in the preliminary experiments revealed an *c.* 80% reduction in *StUBK* transcript accumulation (Fig. S7d). Each of the RNAi lines showed similar, significant enhancement of *P. infestans* colonization ($P < 0.001$, one-way ANOVA; Fig. S8a), which was apparent using trypan blue (Fig. S8b). Three of these RNAi lines were selected (i2-24, i2-32, i2-39) for further analysis as they showed 80–90% reduction in *StUBK* transcript accumulation (Fig. S7d). *Phytophthora infestans* colonization, measured as *P. infestans* biomass, determined by qPCR measurement of pathogen DNA, was significantly ($P < 0.001$, one-way ANOVA) more extensive between 2 and 3 dpi compared with the untransformed cultivar E3 (measured for line i2-39 in Fig. 4d). Moreover, all three lines showed significantly enhanced *P. infestans* colonization, as measured by lesion diameter and number of sporangia (Figs 4e,f, S8b), by stained *P. infestans* mycelia (Bos *et al.*, 2010).

Overexpression of StUBK reduces *P. infestans* leaf colonisation

We investigated the affect of overexpression of StUBK on late blight disease. Critically, transient expression of GFP–StUBK led to significantly ($P < 0.05$, one-way ANOVA) reduced *P. infestans* colonization compared with the GFP control (Fig. 4g). Taken together, the VIGS in *N. benthamiana*, RNAi in potato and overexpression demonstrate that UBK contributes to restricting *P. infestans* infection.

To examine whether overexpression of StUBK has an effect on the virulence activity of PiSFI3, GFP–PiSFI3 was transient expressed in *N. benthamiana* alone or co-expressed with GFP–StUBK and challenged with *P. infestans* spores at 1 dpi, using GFP–EV and GFP–Pi04089 as controls. At 6 dpi, GFP–PiSFI3 or GFP–Pi04089 expressed alone enhanced *P. infestans* colonization to a significant level ($P < 0.001$, one-way ANOVA) compared with the GFP–EV control (Fig. 4h), as anticipated. However, the ability of GFP–PiSFI3 to enhance *P. infestans* colonisation was significantly reduced (ANOVA, $P < 0.5$) by co-expression with GFP–StUBK. By contrast, enhanced colonisation of *P. infestans* by GFP–Pi04089 was unaltered when co-expressed with GFP–StUBK (Fig. 4h). StUBK overexpression was therefore able to specifically reduce PiSFI3 virulence activity.

VIGS of *UBK* does not compromise INF1 or Cf4/Avr4 cell deaths

PiSFI3 attenuates flg22-mediated early transcriptional events, but does not suppress PCD triggered by INF1 or CF4/Avr4. We therefore proceeded to investigate whether PCD triggered in *N. benthamiana* by measurement of INF1, or if CF4/Avr4 requires UBK. Silencing of UBK did not attenuate INF1 or CF4/Avr4 cell death, indicating that UBK is not involved in the cell death responses to INF1 and Avr4 (Fig. S9).

Silencing of *UBK* attenuates early flg22 induced marker genes

PiSFI3 suppressed pFRK:luc reporter induction following flg22 treatment (Zheng *et al.*, 2014, 2018) and suppressed flg22-mediated early gene expression (*NbWRKY7* and *NbACRE31*) in potato (Fig. 2f,g). We investigated whether the expression of *StUBK* also responded to the flg22 treatment. Following flg22 infiltration into leaves (performed as described previously by He *et al.*, 2015 and McLellan *et al.*, 2013), increased *StUBK* transcript accumulation was noted as early as 3 h postinoculation,

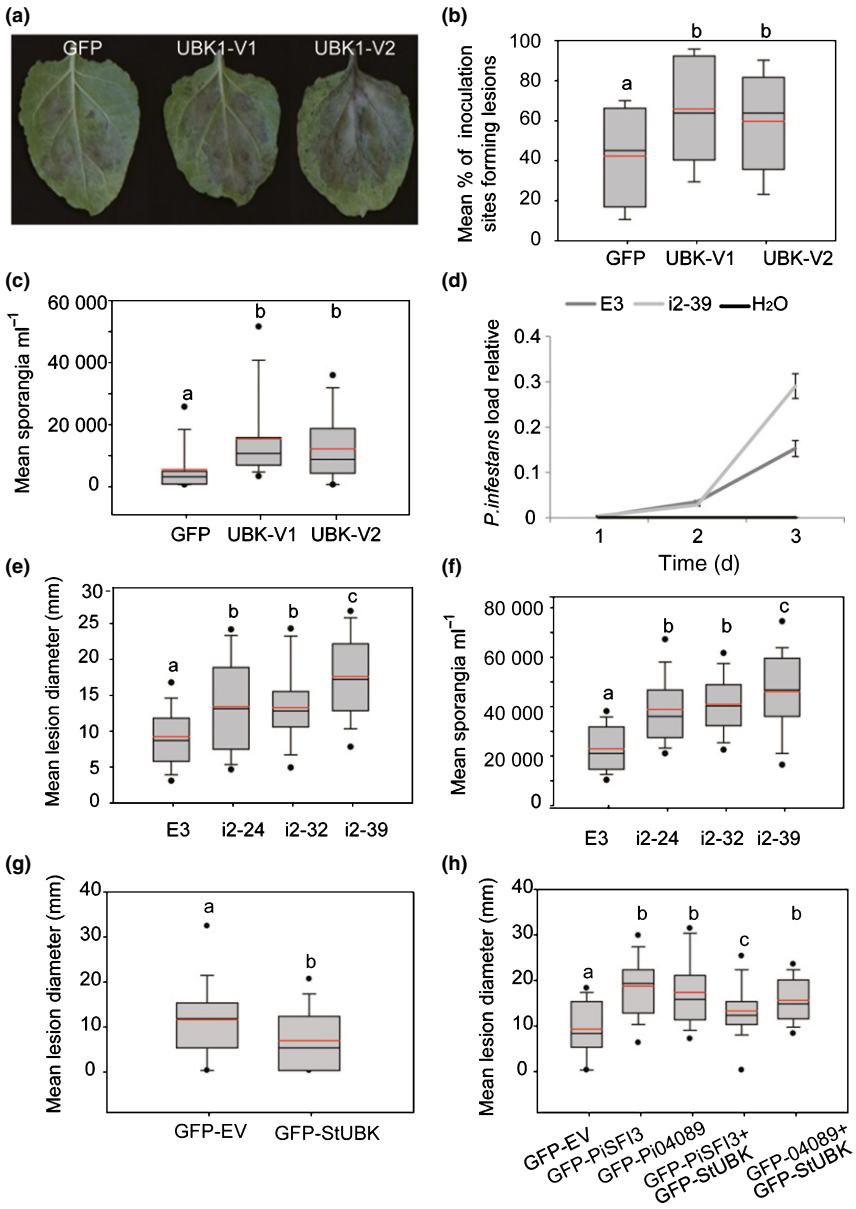

Fig. 4 Silencing of *UBK* enhances, and overexpression reduces, *Phytophthora infestans* leaf colonisation. (a) Representative leaf images show the extent of *P. infestans* leaf colonisation on plants expressing each two independent virus-induced gene silencing (VIGS) constructs (UBK- V1 and UBK- V2) in *Nicotiana benthamiana*. (b) Silencing of UBK using two independent VIGS constructs (UBK-V1 and UBK- V2) in *N. benthamiana* significantly increases *P. infestans* lesion number compared with the GFP control. Boxplots represent the combined data from five biological reps. Letters on the boxplots denote statistically significant differences (ANOVA, $P < 0.001$). (c) Silencing of *UBK* using two independent virus-induced gene silencing (VIGS) constructs allow a significant increase in *P. infestans* sporulation compared with the GFP control. Boxplots represent the combined data from four biological reps ($n = 32$). Letters on the boxplots denote statistically significant differences (ANOVA, $P < 0.05$). (d) Graph shows that silencing *StUBK* by RNAi in potato significantly increases *P. infestans* biomass compared to the GFP control. *Phytophthora infestans* biomass determined by qPCR measurement of pathogen DNA using *Ef-1α* (used to quantify *Solanum tuberosum* DNA) and PiO8 primers (designed based on highly repetitive sequences from the *P. infestans* genome to quantify *P. infestans*. Three leaves for each time point (every 24 h after inoculation with *P. infestans*) were harvested and snap frozen in liquid nitrogen. The DNA was extract and quantified by qRT-PCR. (e) Boxplots show mean *P. infestans* lesion diameter of potato cultivar E3 and transgenic *StUBK* RNAi plants measured at 5 d post inoculation (dpi). Boxplots represent the combined data from three biological reps (34 leaves per line). Letters on the boxplots denote statistically significant differences (ANOVA, $P < 0.001$). (f) Transgenic potato RNAi lines silencing *StUBK* allow a significant increase in *P. infestans* sporulation compared to the E3 control. Boxplots represent the combined data from three biological reps ($n = 96$). Letters on the boxplots denote statistically significant differences (ANOVA, $P < 0.001$). (g) GFP−StUBK following *Agrobacterium*-mediated expression significantly ($P < 0.05$) reduces the ability of *P. infestans* to colonise *N. benthamiana* compared with the GFP−EV control. Lesion size was recorded after 6 d. Boxplots represent the combined data from three biological reps ($n = 78$). (h) GFP−PiSFI3 and GFP−Pi04089 following *Agrobacterium*-mediated expression significantly ($P < 0.001$) enhance *P. infestans* colonization compared to GFP−E control. GFP−StUBK significantly ($P < 0.05$) reduces the ability of GFP−PiSFI3 but not GFP−Pi04089 to colonise *N. benthamiana* compared to GFP−EV control or GFP−PiSFI3. Lesion size was recorded after 6 d. Boxplots represent the combined data from three biological reps ($n = 60$). For each boxplot the black line represents the median and the red line the mean. The black dot above and below each box represent the 95th and 5th percentage of outliers, respectively.

peaking at 6 h (Fig. S10a). This prompted us to investigate whether UBK contributes to the flg22-mediated PTI response, using the early-induced genes *NbWRKY7* and *NbACRE31* as transcriptional markers. Following flg22 treatment of *NbUBK* VIGS plants, *NbWRKY7* and *NbACRE31* transcript accumulation was attenuated compared with the TRV-GFP control (Fig. 5a,b). Similarly, a reduced accumulation of *StWRKY7* and *StACRE31* transcripts was observed in the three RNAi lines of *StUBK* (i2-24, i2-32, i2-39) compared with the untransformed potato cultivar E3 control (Figs 5c,d, S10b,c). This indicates that UBK contributes to the flg22-triggered PTI transcriptional response.

PiSFI3 is a WY-domain RXLR effector with a *trans*-homodimer fold

To investigate how PiSFI3 may function at the molecular level, we determined its crystal structure to 1.7 Å resolution (Table S2). The PiSFI3 structure comprises residues Ala^{63}–Lys^{117} of the full-length sequence and adopts an antiparallel extended α-helical fold (Fig. 6a). The structure confirms that SFI3 adopts the 'WY-domain' fold, as previously predicted (Boutemy *et al.*, 2011). However, unlike previous structures of RXLR effectors, PiSFI3 forms a novel '*trans*' WY-domain configuration in which the 'W' (Trp) and 'Y' (Tyr) residues are derived from separate monomers (Fig. 6a). Therefore, the SFI3 structure further highlights the adaptability of the WY-domain to form diverse conformations (Winn *et al.*, 2011; Maqbool *et al.*, 2016, Fig. S11a). To test whether PiSFI3 can oligomerise *in planta* we used Co-IP with cMYC- and mRFP-tagged versions of the protein co-expressed in *N. benthamiana* (Fig. 6b). Following immunoprecipitation with anti-mRFP antibodies we detected cMYC–PiSFI3 protein in samples where mRFP–PiSFI3 was co-expressed, but not the mRFP–GUS control, confirming that PiSFI3 can oligomerise in plant cells (Fig. 6b).

We then examined the PiSFI3 structure to identify amino acid residues that, on mutation, might perturb protein structure and inform functional studies. For this we chose to generate the double mutants $PiSFI3^{L86D/L100D}$ and $PiSFI3^{L86D/L103D}$. These pairs of residues faced each other across the PiSFI3 α-helices and Leu/Asp mutations would be predicted to result in conformational changes in the protein, potentially disrupting oligomerisation (Fig. 6a). Indeed, whereas mRFP–PiSFI3 co-immunoprecipitated cMYC–PiSFI3, co-immunoprecipitation of cMYC–$PiSFI3^{L86D/L100D}$ and cMYC–$PiSFI3^{L86D/L103D}$ by, respectively, mRFP–$PiSFI3^{L86D/L100D}$ and mRFP–$PiSFI3^{L86D/L103D}$ was attenuated (Figs 6b, S11b).

Structure-guided mutations of SFI3 are attenuated in virulence function and lose nucleolar localisation

As shown above, nuclear/nucleolar localization of GFP–PiSFI3 is important for *P. infestans* virulence. To determine the subcellular localization of GFP–$PiSFI3^{L86D/L100D}$ and GFP–$PiSFI3^{L86D/L103D}$, we transiently expressed these mutants in *N. benthamiana* alongside GFP–PiSFI3 as a positive control. As previously observed, GFP–PiSFI3 accumulated strongly in the nucleus, forming a ring around the nucleolus, with additional cytoplasmic background (Fig. 7a). By contrast, GFP–$PiSFI3^{L86D/L100D}$ and GFP–$PiSFI3^{L86D/L103D}$ fluorescence was primarily in the nucleoplasm, with cytoplasmic background, and was reduced in the nucleolus, leading to a

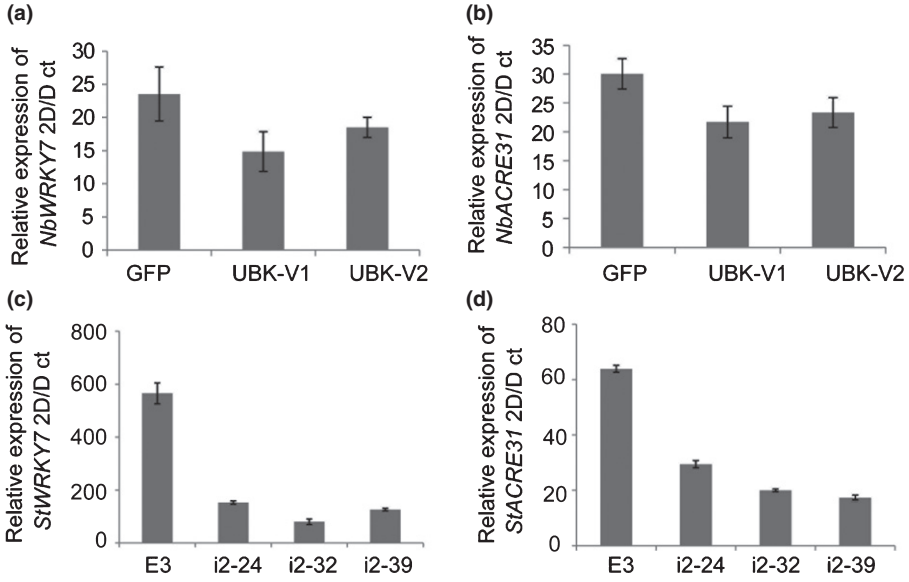

Fig. 5 Silencing of *UBK* attenuates early flg22 induced marker genes. (a, b) Relative expression of flg22 marker genes *NbWRKY7* and *NbACRE31* 3 h after treatment with flg22 in GFP, and UBK VIGS plants (UBK-V1 and UBK-V2). (c, d) Relative expression of flg22 marker genes *StWRKY7* and *StACRE31* 30 min after treatment with flg22 in E3, StUBK RNAi lines (i2-24, i2-32, i2-39). Error bars represent ± SE. RNA was extracted to synthesis cDNA and qRT-PCR reactions were performed using Power SYBR Green for gene expression assays. Primers used are available in Supporting Information Table S1. Relative expression of the target genes was calculated using the $2^{\Delta\Delta Ct}$ method with the StUBI housekeeping gene as the reference for potato as described previously (Livak & Schmittgen, 2001; McLellan *et al.*, 2013).

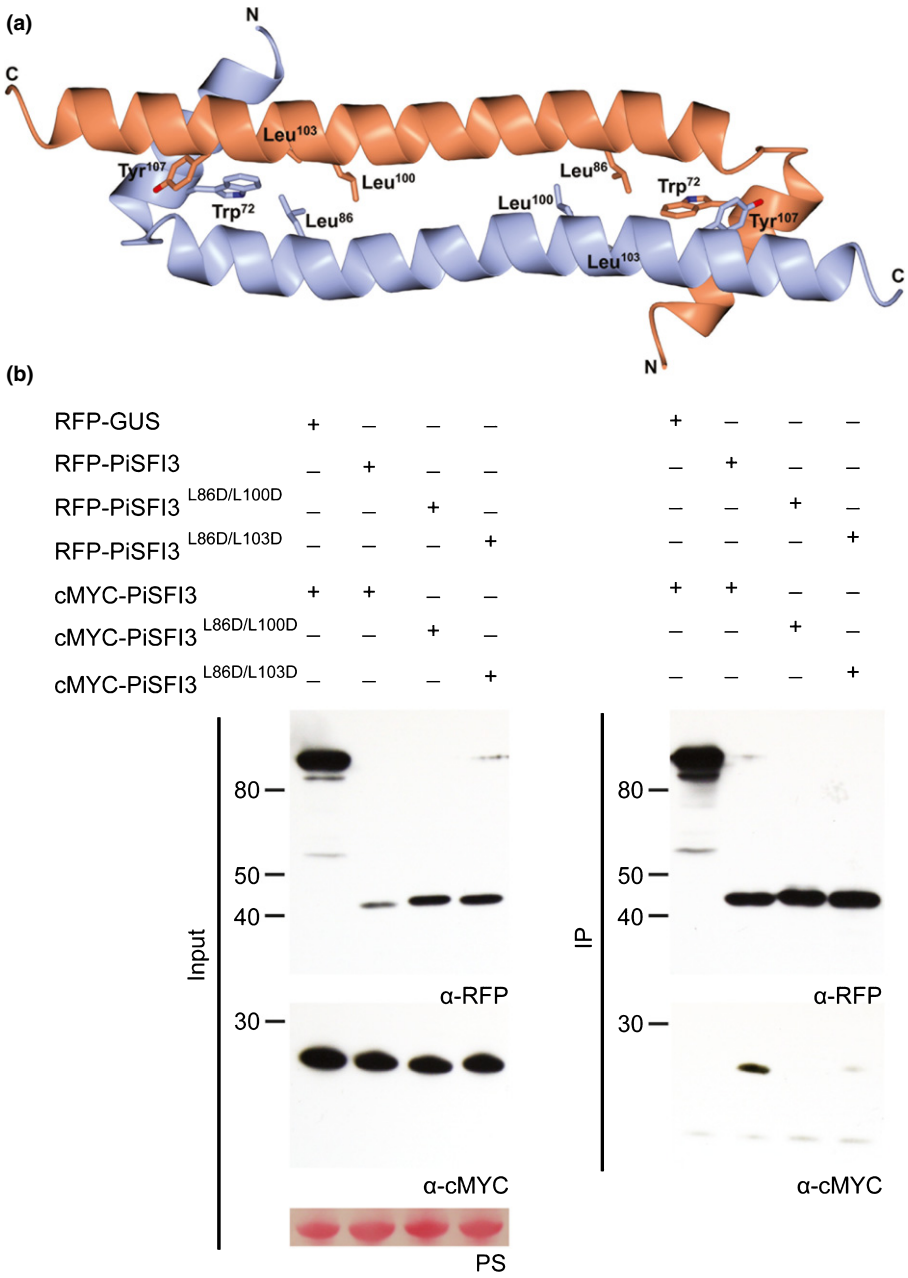

Fig. 6 SFI3 forms a homodimer with an unusual '*trans*-WY' configuration and self-associates *in planta*. (a) Overall schematic view of the crystal structure of SFI3. SFI3 comprises two extended helical folds (monomers coloured blue and orange) that form a dimer in a '*trans*-WY' configuration. The positions of the N- and C-termini, Trp^{72} and Tyr^{107}, and of the Leu residues (Leu^{86}, Leu^{100} and Leu^{103}) that were mutated to disrupt dimer formation, are labelled in each monomer and shown with side chains in stick representation. Structure figures were prepared with CCP4MG (McNicholas *et al.*, 2011). (b) SFI3 can oligomerise *in planta* by Co-IP. cMYC- and mRFP-tagged versions of the proteins co-expressed in *Nicotiana benthamiana*. Following immunoprecipitation with anti-mRFP antibodies, cMYC-tagged PiSFI3 protein in samples where mRFP–PiSFI3 has been expressed, but not the mRFP–GUS control, confirming PiSFI3 can oligomerise in plant cells. Co-immunoprecipitation of cMYC–$PiSFI3^{L86D/L100D}$ and cMYC–$PiSFI3^{L86D/L103D}$ by, respectively, mRFP–$PiSFI3^{L86D/L100D}$ and mRFP–$PiSFI3^{L86D/L103D}$ was attenuated. Expression of constructs in the leaves is indicated by +. Protein size markers are indicated in kDa, and protein loading is indicated by Ponceau stain (PS).

significantly reduced ratio of nucleolar-to-nucleoplasmic fluorescence (Figs 7a,b, S12). GFP–PiSFI3, GFP–$PiSFI3^{L86D/L100D}$ and GFP–$PiSFI3^{L86D/L103D}$ fusions were stable *in planta* (Fig. S12).

As expression of PiSFI3 *in planta* enhances infection (Fig. 1), we tested whether the mutations altered effector virulence function. GFP–PiSFI3, GFP–$PiSFI3^{L86D/L100D}$ or GFP–$PiSFI3^{L86D/L103D}$ were transiently expressed in one-half of an *N. benthamiana* leaf with empty GFP expressed as a control in the other. The two halves of the leaves were drop-inoculated with *P. infestans* zoospores and lesion size was measured at 6 d postinoculation. Unlike the wild-type GFP–PiSFI3, both GFP–$PiSFI3^{L86D/L100D}$ and GFP–$PiSFI3^{L86D/L103D}$ failed to enhance *P. infestans* colonization, and each showed no significant difference compared with a GFP–EV control (ANOVA, $P < 0.001$; Figs 7c, S12c).

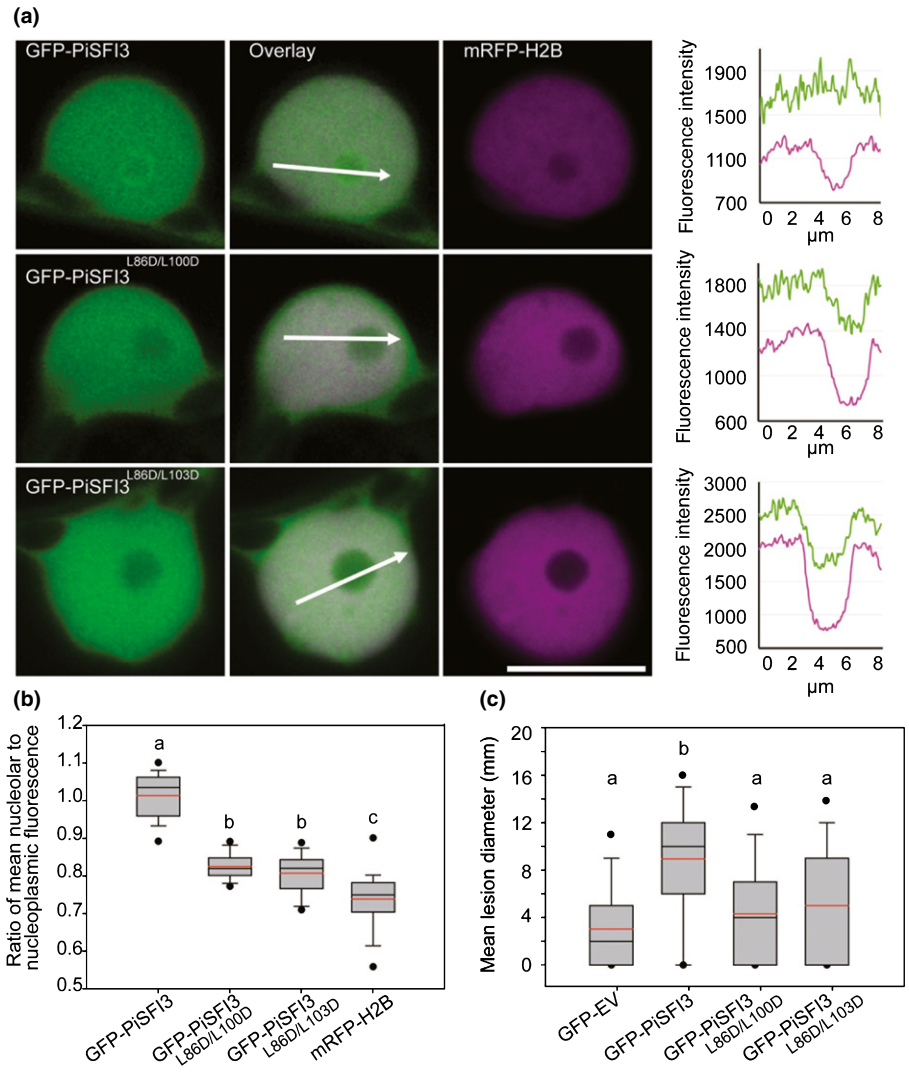

Fig. 7 SFI3 mutants lose nucleolar localisation and are attenuated in virulence function. (a) Image sets are single optical sections of typical nuclei co-expressing GFP–PiSFI3 or the GFP–PiSFI3$^{L86D/L100D}$ or GFP–PiSFI3$^{L86D/L103D}$ with the nuclear marker *Nicotiana benthamiana* histone H2B fused to mRFP (mRFP–H2B). Bar, 10 mm. White arrows indicate GFP (green) and mRFP (red) fluorescence intensity plots shown in graphs to the right of each image. (b) Graph of the ratio of nucleolar to nucleoplasmic mean fluorescence intensity in nuclei of cells expressing GFP–PiSFI3, PiSFI3$^{L86D/L100D}$ or PiSFI3$^{L86D/L103D}$ shows the reduction in nucleolar association of the mutant forms of the effector. The ratio for the nuclear marker *N. benthamiana* histone H2B fused to mRFP (mRFP–H2B) is included for comparison. A minimum of 25 nuclei was measured for each construct. Error bars show SE. (c) Expression of wild-type GFP–PiSFI3 significantly enhances *Phytophthora infestans* infection compared with the control GFP–EV. However, the PiSFI3 mutants GFP–PiSFI3$^{L86D/L100D}$ and GFP–PiSFI3$^{L86D/L103D}$ fail to enhance *P. infestans* colonisation. Boxplots represent the combined data from three biological reps ($n = 129$ leaves per construct). Letters on the boxplots denote statistically significant differences (ANOVA, $P < 0.001$). The black line represents the median and the red line the mean. The black dot above and below each box represent the 95th and 5th percentage of outliers, respectively.

PiSFI3 mutations prevent interaction with StUBK

As PiSFI3 mutations showed reduced virulence activity, this prompted us to investigate whether the mutations had an effect on the interaction with StUBK. StUBK was cloned into the Y2H prey construct and tested pairwise with bait constructs containing PiSFI3, PiSFI3$^{L86D/L100D}$ and PiSFI3$^{L86D/L103D}$ along with a control RXLR effector (Pi04089). Whereas all transformants grew on the control plates (+HIS), only yeast containing both PiSFI3 and StUBK was able to grow on the selection (−HIS) plates and activate the β-galactosidase (β-GAL) reporter (Fig. 8a). The result indicates that PiSFI3$^{L86D/L100D}$ and PiSFI3$^{L86D/L103D}$ failed to interact with StUBK in a Y2H assay.

To further investigate the interaction between StUBK and the two mutants *in planta*, RFP-tagged StUBK was used in co-immunoprecipitation experiments. cMYC–PiSFI3, cMYC–PiSFI3$^{L86D/L100D}$ and cMYC–PiSFI3$^{L86D/L103D}$ were co-expressed in *N. benthamiana* with N-terminal RFP-tagged StUBK, respectively, with cMYC–GUS used as a noninteracting control. All constructs were detected in the relevant input fractions. Following immunoprecipitation using RFP–TRAP_M beads, only the cMYC–SFI3 construct, and not the cMYC–PiSFI3$^{L86D/L100D}$ or cMYC–PiSFI3$^{L86D/L103D}$, was detected in the presence of RFP-UBK (Fig. 8b), confirming that PiSFI3$^{L86D/L100D}$ and PiSFI3$^{L86D/L103D}$ fail to interact with StUBK *in planta*.

Discussion

The RXLR effector PiSFI3 acts downstream of MAP kinase activation to suppress flg22-triggered transcriptional defence responses (Zheng *et al.*, 2014, 2018). Here we show that PiSFI3 forms a *trans*-homodimer that targets a plant protein that uniquely contains both U-box and kinase domains (StUBK). StUBK is a positive regulator specifically of early transcriptional changes that can be triggered by the bacterial MAMP flg22.

Transient expression of GFP–PiSFI3 in *N. benthamiana* enhanced colonization by *P. infestans* (Zheng *et al.*, 2014, 2018). Although future work to silence expression of *PiSFI3* in *P. infestans* may reveal whether this effector is essential for infection, we

demonstrate that its stable transgenic expression in potato resulted in enhanced *P. infestans* leaf colonization, supporting its role as an effector (Fig. 2). Moreover, transgenic PiSFI3-expressing potato lines attenuate early flg22-mediated transcriptional gene expression in agreement with the previous assay reported in tomato protoplasts (Zheng *et al.*, 2014, 2018). As *P. infestans* does not possess the MAMP flagellin, the ability of PiSFI3 to attenuate flg22-triggered early defences indicates that the receptor FLS2 activates a generic signal transduction pathway that is likely to be also activated by an unknown receptor that detects an oomycete MAMP (Zheng *et al.*, 2014, 2018). It will be interesting to identify both the host receptor(s) and *P. infestans* elicitor(s) responsible for activating this defence pathway in future work.

Suppression of flg22-triggered transcriptional responses by PiSFI3 is mediated by its interaction with StUBK. We show that silencing *UBK* in both potato and *N. benthamiana* attenuates flg22-triggered transcriptional responses (Fig. 5). This silencing leads to increased *P. infestans* susceptibility, whereas overexpression of StUBK increases resistance to *P. infestans* (Fig. 4). Critically, co-expression of StUBK with either PiSFI3 or the control effector Pi04089 specifically attenuated the virulence activity of the former (Fig. 4), providing evidence that UBK is the likely operative target of SFI3. Further genetic evidence indicating this to be the case was provided by mutation of PiSFI3 that linked its ability to interact with StUBK with its ability to enhance *P. infestans* colonisation (Figs 7, 8). Interestingly, PiSFI3 overexpression or *UBK* silencing had no impact upon cell death triggered by perception of the *P. infestans* MAMP INF1 (Figs S4, S9), suggesting that effector and target are specific to a particular defence pathway. Future work will investigate whether INF1 activates early transcriptional responses in common with flg22 perception that led to defences other than cell death, and which are suppressed by PiSFI3.

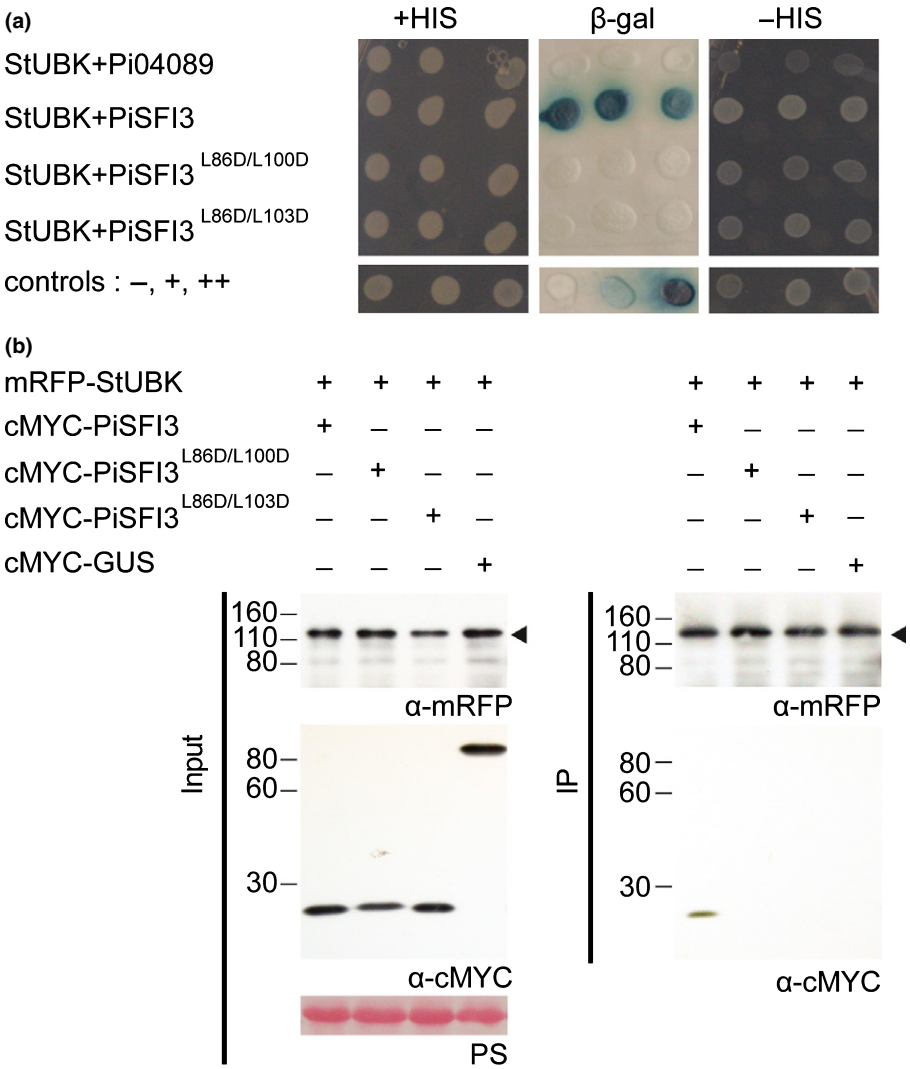

Fig. 8 Structure-guided mutation of SFI3 prevents its interaction with UBK. (a) Yeast co-expressing StUBK with PiSFI3 grew on −histidine (−HIS) medium and yielded β-galactosidase (β-Gal) activity, while those co-expressed with the control Pi04089, PiSFI3$^{L86D/L100D}$, or PiSFI3$^{L86D/L103D}$ did not. The +HIS control shows all yeast were able to grow in the presence of histidine. (b) These interactions were further confirmed by co-immunoprecipitation (Co-IP) assay using protein extracted from agroinfiltrated *Nicotiana benthamiana* leaves. cMYC−PiSFI3 associated with mRFP−StUBK, whereas cMYC−GUS, cMYC−PiSFI3$^{L86D/L100D}$, or cMYC−PiSFI3$^{L86D/L103D}$ did not. Expression of constructs in the leaves is indicated by +. Protein size markers are indicated in kDa, and protein loading is indicated by Ponceau stain (PS). The arrowheads show the RFP-tagged fusion proteins.

PiSFI3 localizes to the host nucleus, forming a ring around the nucleolus, with additional cytoplasmic background. The virulence activity of the effector was considerably reduced when it was directed away from the nucleus with a nuclear export signal (NES), suggesting that the nucleus is an important site of PiSFI3 action. In agreement, when PiSFI3 was focused in the nucleus with an NLS, the beneficial activity of the effector was not diminished (Fig. 1). While background levels of the $_{NLS}$GFP–PiSFI3 fusion may yet remain in the cytoplasm, we argue that the lack of a statistically significant change to enhanced *P. infestans* colonization by the effector suggests that a cytoplasmic stage is not critical for PiSFI3 function. We therefore conclude that PiSFI3 activity is primarily in the nucleus. This is further supported by two observations. Firstly, StUBK was also present in the nucleolus, again forming a ring around this nuclear structure (Fig. 3). Moreover, mutations of PiSFI3 that disrupt its dimerization, prevent its interaction with StUBK, and attenuate its virulence function, also result in its failure to accumulate in the nucleolus (Fig. 7). Whilst these mutant forms still reside in the nucleoplasm, their failure to form a ring around the nucleolus or accumulate within it, strongly implicates this as the primary site of activity. It is interesting to note that both CMPG1 (Gilroy *et al.*, 2011) and PUB17 (He *et al.*, 2015) accumulate also in the nucleolus. Future work will reveal more about the function of StUBK in the nucleus by combining mutations of the U-box and kinase domains in the protein with studies to mis-direct it away from the nucleus or to exclusively localise it there using an NLS.

PiSFI3 adopts the 'WY-domain' fold, as previously predicted (Boutemy *et al.*, 2011). However, unlike previous structures of RXLR effectors, SFI3 forms a novel '*trans*' WY-domain configuration that can oligomerise *in vitro*. We demonstrate that PiSFI3 also oligomerises *in planta*. Mutation of Leu/Asp pairs of residues (L86D/L100D, L86D/L103D) that face each other across the PiSFI3 α-helices resulted in conformational changes that disrupted oligomerisation (Fig. 6). Interestingly, we found that the two mutants (PiSFI3$^{L86D/L100D}$ and PiSFI3$^{L86D/L103D}$) that were stable *in planta* but no longer accumulated in the nucleolus, interacted with StUBK, or enhanced *P. infestans* colonisation. This demonstrates that the *trans*-homodimer is biologically relevant, and highlights the flexibility of the WY-domain fold.

Plant kinases and E3 ubiquitin ligases are well known for their functions in a variety of stress responses. Both phosphorylation and ubiquitination can either positively or negatively regulate immunity (Mithoe & Menke, 2018; Trujillo, 2018). StUBK possesses both a kinase domain and a U-box domain, indicating that it potentially regulates immunity via these PTMs. Both kinases and E3 ligases are targeted by pathogen effectors, either to prevent their activity, or potentially to utilise it. For example, PexRD2 suppresses the kinase signalling activity of its target MAP3Kε (King *et al.*, 2014) to prevent phosphorylation of its substrates. More recently, *P. infestans* effector Pi17316 has been shown to target the MAP3K StVIK, utilising or promoting its activity as an S factor to suppress immunity (Murphy *et al.*, 2018). Similarly, whereas the *P. infestans* effector AVR3a targets the E3 ligase CMPG1 to prevent its normal function (Bos *et al.*, 2010), and effector Avr-Piz-t from *Magnaporthe oryzae* directly interacts with E3 ligases APIP6 and APIP10 to inhibit their positive regulation of PTI (Park *et al.*, 2012, 2016), the effector Pi02860 from *P. infestans* utilizes host susceptibility factor E3 ligase NRL1 to degrade the immune regulator SWAP70 (Yang *et al.*, 2016; He *et al.*, 2018). Presumably, PiSFI3 prevents the normal activity of StUBK. Indeed, this is supported by observation that the effector attenuates the specific immune pathway that is activated by StUBK. Further work is needed to determine whether PiSFI3 inhibits either phosphorylation or ubiquitination activities, or interferes with substrate specificity of StUBK.

There is considerable cross-talk between ubiquitination and phosphorylation in the regulation of immunity. Phosphorylation often serves as a marker that triggers subsequent ubiquitination, in particular when ubiquitination leads to degradation. In other cases, ubiquitination provide a switching mechanism that can turn on/off the kinase activity of certain proteins. One recurrent theme for PUB E3 ligases is their interaction with kinase domains (Trujillo, 2018). For example, the kinase FLS2 is a target for ubiquitination and turnover by PUB13 (Lu *et al.*, 2011). In addition, it was reported that U-box E3 ligase PUB13 regulates the abundance of chitin receptor LYK5 protein (Lysine Motif-Receptor-Like Kinase 5) that is required for the activation of the CERK1 intracellular kinase domain and induction of plant innate immunity (Cao *et al.*, 2014; Liao *et al.*, 2017). Moreover, some positive regulators of immune pathways that act at the transcriptional level, such as the JA regulator MYC2, are both activated by phosphorylation and immediately inactivated by ubiquitination (Zhai *et al.*, 2013). Turnover of phosphorylated NPR1 is required for full induction of target genes and establishment of systemic acquired resistance (SAR; Spoel *et al.*, 2009). It is therefore perhaps unsurprising that StUBK, a positive regulator of immunity at the transcriptional level, contains both E3 ligase and kinase domains. Understanding how these two major PTMs interact to regulate signal transduction is an important topic in characterization of StUBK function in plant immunity. Future work will aim to uncover the details surrounding the interplay between phosphorylation and ubiquitination in StUBK and how this regulation is controlled upon *P. infestans* perception in the regulation of immune gene transcription. Of particular interest will be the identification of substrates for each PTM. A knowledge of these substrates will not only reveal how StUBK works, but will allow us also to fully understand the mode-of-action of PiSFI3 in targeting it to suppress early PTI transcriptional responses.

Acknowledgements

We are grateful for financial support from the Biotechnology and Biological Sciences Research Council (BBSRC) (grants BB/G015244/1, BB/K018183/1, BB/L026880/1, BB/P020569/1), the Scottish Government Rural and Environment Science and Analytical Services Division (RESAS), and the National Natural Science Foundation of China (grants 31171603, 31471550), the National High Technology Research and Development Program of China (grant 2013AA102603), and the Fundamental Research Funds for the Central Universities of China (grant 2662017PY069).

Author contributions

PRJB, MJB, QH and ZT planned and designed the research. QH, HM, RKH, PCB, MA and YL, performed experiments and analysed data. QH, PRJB and MJB wrote the manuscript with input from all authors.

ORCID

Miles Armstrong https://orcid.org/0000-0002-9441-476X
Mark J. Banfield https://orcid.org/0000-0001-8921-3835
Paul R. J. Birch https://orcid.org/0000-0002-6559-3746
Petra C. Boevink https://orcid.org/0000-0002-7021-9097
Qin He https://orcid.org/0000-0002-4957-2785
Richard K. Hughes https://orcid.org/0000-0001-9910-6566
Yuan Lu https://orcid.org/0000-0001-6313-2578
Hazel McLellan https://orcid.org/0000-0003-4490-7053
Zhendong Tian https://orcid.org/0000-0002-3271-5372

References

Ah-Fong AM, Kim KS, Judelson HS. 2017. RNA-seq of life stages of the oomycete *Phytophthora infestans* reveals dynamic changes in metabolic, signal transduction, and pathogenesis genes and a major role for calcium signaling in development. *BMC Genomics* **18**: 198.

Berrow NS, Alderton D, Sainsbury S, Nettleship J, Assenberg R, Rahman N, Stuart DI, Owens RJ. 2007. A versatile ligation-independent cloning method suitable for high-throughput expression screening applications. *Nucleic Acids Research* **35**: e45.

Boevink PC, McLellan H, Gilroy EM, Naqvi S, He Q, Yang L, Wang X, Turnbull D, Armstrong MR, Tian Z *et al.* 2016a. Oomycetes seek help from the plant: *Phytophthora infestans* effectors target host susceptibility Factors. *Molecular Plant* **9**: 636–638.

Boevink PC, Wang X, McLellan H, He Q, Naqvi S, Armstrong MR, Zhang W, Hein I, Gilroy EM, Tian Z *et al.* 2016b. A *Phytophthora infestans* RXLR effector targets plant PP1c isoforms that promote late blight disease. *Nature Communications* **7**: 10311.

Bos JIB, Armstrong MR, Gilroy EM, Boevink PC, Hein I, Taylor RM, Tian ZD, Engelhardt S, Vetukuri RR, Harrower B *et al.* 2010. *Phytophthora infestans* effector Avr3a is essential for virulence and manipulates plant immunity by stabilizing host E3 ligase CMPG1. *Proceedings of the National Academy of Sciences, USA* **107**: 9909–9914.

Boutemy LS, King SR, Win J, Hughes RK, Clarke TA, Blumenschein TM, Kamoun S, Banfield MJ. 2011. Structures of Phytophthora RXLR effector proteins: a conserved but adaptable fold underpins functional diversity. *Journal of Biological Chemistry* **286**: 35834–35842.

Cao Y, Liang Y, Tanaka K, Nguyen CT, Jedrzejczak RP, Joachimiak A, Stacey G. 2014. The kinase LYK5 is a major chitin receptor in Arabidopsis and forms a chitin-induced complex with related kinase CERK1. *eLife* **3**. doi: 10.7554/eLife.03766.

Chen VB, Arendall WB III, Headd JJ, Keedy DA, Immormino RM, Kapral GJ, Murray LW, Richardson JS, Richardson DC. 2010a. MolProbity: all-atom structure validation for macromolecular crystallography. *Acta Crystallographica. Section D, Biological Crystallography* **66**: 12–21.

Chen Y, Hoehenwarter W, Weckwerth W. 2010b. Comparative analysis of phytohormone-responsive phosphoproteins in *Arabidopsis thaliana* using TiO2-phosphopeptide enrichment and mass accuracy precursor alignment. *The Plant Journal* **63**: 1–17.

Cooke DE, Cano LM, Raffaele S, Bain RA, Cooke LR, Etherington GJ, Deahl KL, Farrer RA, Gilroy EM, Goss EM, *et al.* 2012. Genome analyses of an aggressive and invasive lineage of the Irish potato famine pathogen. *PLoS Pathogens* **8**: e1002940.

Emsley P, Lohkamp B, Scott WG, Cowtan K. 2010. Features and development of COOT. *Acta Crystallographica. Section D, Biological Crystallography* **66**: 486–501.

Filipčík P, Curry JR, Mace PD. 2017. When Worlds Collide-Mechanisms at the interface between phosphorylation and ubiquitination. *Journal of Molecular Biology* **429**: 1097–1113.

Fry WE, Birch PRJ, Judelson HS, Grünwald NJ, Danies G, Everts KL, Gevens AJ, Gugino BK, Johnson DA, Johnson SB *et al.* 2015. Five Reasons to Consider *Phytophthora infestans* a Reemerging Pathogen. *Phytopathology* **105**: 966–981.

Gilroy EM, Hein I, van der Hoorn R, Boevink PC, Venter E, McLellan H, Kaffarnik F, Hrubikova K, Shaw J, Holeva M *et al.* 2007. Involvement of cathepsin B in the plant disease resistance hypersensitive response. *The Plant Journal* **52**: 1–13.

Gilroy EM, Taylor RM, Hein I, Boevink P, Sadanandom A, Birch PRJ. 2011. CMPG1-dependent cell death follows perception of diverse pathogen elicitors at the host plasma membrane and is suppressed by *Phytophthora infestans* RXLR effector Avr3a. *New Phytologist* **190**: 653–666.

Haas BJ, Kamoun S, Zody MC, Jiang RHY, Handsaker RE, Cano LM, Grabherr M, Kodira CD, Raffaele S, Torto-Alalibo T *et al.* 2009. Genome sequence and analysis of the Irish potato famine pathogen *Phytophthora infestans*. *Nature* **461**: 393–398.

He Q, McLellan H, Boevink PC, Sadanandom A, Xie C, Birch PR, Tian Z. 2015. U-box E3 ubiquitin ligase PUB17 acts in the nucleus to promote specific immune pathways triggered by *Phytophthora infestans*. *Journal of Experimental Botany* **66**: 3189–3199.

He Q, Naqvi S, McLellan H, Boevink PC, Champouret N, Hein I, Birch PRJ. 2018. Plant pathogen effector utilizes host susceptibility factor NRL1 to degrade the immune regulator SWAP70. *Proceedings of the National Academy of Sciences, USA* **115**: E7834–E7843.

Ishihama N, Yoshioka H. 2012. Post-translational regulation of WRKY transcription factors in plant immunity. *Current Opinion in Plant Biology* **15**: 431–437.

Jones JD, Dangl JL. 2006. The plant immune system. *Nature* **444**: 323–329.

Kamoun S, Furzer O, Jones JD, Judelson HS, Ali GS, Dalio RJ, Roy SG, Schena L, Zambounis A, Panabières F *et al.* 2015. The Top 10 oomycete pathogens in molecular plant pathology. *Molecular Plant Pathology* **16**: 413–434.

King SR, McLellan H, Boevink PC, Armstrong MR, Bukharova T, Sukarta O, Win J, Kamoun S, Birch PRJ, Banfield MJ. 2014. *Phytophthora infestans* RXLR effector PexRD2 interacts with host MAPKKKε to suppress plant immune signaling. *Plant Cell* **26**: 1345–1359.

Kong L, Cheng J, Zhu Y, Ding Y, Meng J, Chen Z, Xie Q, Guo Y, Li J, Yang S *et al.* 2015. Degradation of the ABA co-receptor ABI1 by PUB12/13 U-box E3 ligases. *Nature Communications* **6**: 8630.

Liao D, Cao Y, Sun X, Espinoza C, Nguyen CT, Liang Y, Stacey G. 2017. Arabidopsis E3 ubiquitin ligase PLANT U-BOX13 (PUB13) regulates chitin receptor LYSIN MOTIF RECEPTOR KINASE5 (LYK5) protein abundance. *New Phytologist* **4**: 1646–1656.

Liu Y, Schiff M, Dinesh-Kumar SP. 2002. Virus-induced gene silencing in tomato. *The Plant Journal* **31**: 777–786.

Livak KJ, Schmittgen TD. 2001. Analysis of relative gene expression data using real time quantitative PCR and the $2^{-\Delta\Delta C}{}_{T}$ Method. *Methods* **25**: 402–408.

Llorente B, Bravo-Almonacid F, Cvitanich C, Orlowska E, Torres HN, Flawiá MM, Alonso GD. 2010. A quantitative real-time PCR method for in planta monitoring of *Phytophthora infestans* growth. *Letters in Applied Microbiology* **51**: 603–610.

Lu D, Lin W, Gao X, Wu S, Cheng C, Avila J, Heese A, Devarenne TP, He P, Shan L. 2011. Direct ubiquitination of pattern recognition receptor FLS2 attenuates plant innate immunity. *Science* **332**: 1439–1442.

Maqbool A, Hughes RK, Dagdas YF, Tregidgo N, Zess E, Belhaj K, Round A, Bozkurt TO, Kamoun S, Banfield MJ. 2016. Structural basis of host Autophagy-related Protein 8 (ATG8) binding by the Irish potato famine pathogen effector protein PexRD54. *Journal of Biological Chemistry* **291**: 20270–20282.

McLellan H, Boevink PC, Armstrong MR, Pritchard L, Gomez S, Morales J, Whisson SC, Beynon JL, Birch PRJ. 2013. An RxLR effector from *Phytophthora infestans* prevents re-localisation of two plant NAC transcription

factors from the endoplasmic reticulum to the nucleus. *PLoS Pathogens* **9**: e1003670.

McNicholas S, Potterton E, Wilson KS, Noble MEM. 2011. Presenting your structures: the CCP4mg molecular graphics software. *Acta Crystallographica. Section D, Biological Crystallography* **67**: 386–394.

Mithoe SC, Menke FLH. 2018. Regulation of pattern recognition receptor signalling by phosphorylation and ubiquitination. *Current Opinion in Plant Biology* **45**: 162–170.

Murphy F, He Q, Armstrong M, Giuliani LM, Boevink PC, Zhang W, Tian Z, Birch PRJ, Gilroy EM. 2018. Potato MAP3K StVIK is required for *Phytophthora infestans* RXLR effector Pi17316 to promote disease. *Plant Physiology* **177**: 398–410.

Murshudov GN, Vagin AA, Dodson EJ. 1997. Refinement of macromolecular structures by the maximum-likelihood method. *Acta Crystallographica. Section D, Biological Crystallography* **53**: 240–255.

Nguyen LK, Kolch W, Kholodenko BN. 2013. When ubiquitination meets phosphorylation: a systems biology perspective of EGFR/MAPK signalling. *Cell Communication and Signaling* **11**: 52.

Oh SK, Young C, Lee M, Oliva R, Bozkurt TO, Cano LM, Win J, Bos JI, Liu HY, van Damme M *et al.* 2009. *In Planta* expression screens of *Phytophthora infestans* RXLR effectors reveal diverse phenotypes, including activation of the *Solanum bulbocastanum* disease resistance protein Rpi-blb2. *Plant Cell* **21**: 2928–2947.

Orosa B, He Q, Mesmar J, Gilroy EM, McLellan H, Yang C, Craig A, Bailey M, Zhang C, Moore JD *et al.* 2017. BTB-BACK domain protein POB1 suppresses immune cell death by targeting ubiquitin E3 ligase PUB17 for degradation. *PLoS Genetics* **13**: e10065407.

Park CH, Chen S, Shirsekar G, Zhou B, Khang CH, Songkumarn P, Afzal AJ, Ning Y, Wang R, Bellizzi M *et al.* 2012. The *Magnaporthe oryzae* effector AvrPiz-t targets the RING E3 ubiquitin ligase APIP6 to suppress pathogen-associated molecular pattern-triggered immunity in rice. *Plant Cell* **24**: 4748–4762.

Park CH, Shirsekar G, Bellizzi M, Chen S, Songkumarn P, Xie X, Shi X, Ning Y, Zhou B, Suttiviriya P *et al.* 2016. The E3 Ligase APIP10 connects the effector AvrPiz-t to the NLR receptor Piz-t in rice. *PLoS Pathogens* **12**: e1005529.

Rehmany AP, Gordon A, Rose LE, Allen RL, Armstrong MR, Whisson SC, Kamoun S, Tyler BM, Birch PRJ, Beynon JL. 2005. Differential recognition of highly divergent downy mildew avirulence gene alleles by RPP1 resistance genes from two Arabidopsis lines. *Plant Cell* **17**: 1839–1850.

Si HJ, Xie CH, Liu J. 2003. An efficient protocol for *Agrobacterium*-mediated transformation with microtuber and the introduction of an antisense class I *patatin* gene into potato. *Acta Agronomica Sinica* **29**: 801–805.

Spoel SH, Mou Z, Tada Y, Spivey NW, Genschik P, Dong X. 2009. Proteasome-mediated turnover of the transcription coactivator NPR1 plays dual roles in regulating plant immunity. *Cell* **137**: 860–872.

Stegmann M, Anderson RG, Ichimura K, Pecenkova T, Reuter P, Žárský V, McDowell JM, Shirasu K, Trujillo M. 2012. The ubiquitin ligase PUB22 targets a subunit of the exocyst complex required for PAMP-triggered responses in Arabidopsis. *Plant Cell* **24**: 4703–4716.

Trujillo M. 2018. News from the PUB: plant U-box type E3 ubiquitin ligases. *Journal of Experimental Botany* **69**: 371–384.

Wang J, Wang S, Hu K, Yang J, Xin X, Zhou W, Fan J, Cui F, Mou B, Zhang S *et al.* 2018. The kinase OsCPK4 regulates a buffering mechanism that fine-tunes innate immunity. *Plant Physiology* **176**: 1835–1849.

Wang X, Boevink PC, McLellan M, Armstrong M, Bukharova T, Qin Z, Birch PRJ. 2015. A host KH RNA binding protein is a susceptibility factor targeted by an RXLR effector to promote late blight disease. *Molecular Plant* **8**: 1385–1395.

Wawra S, Trusch F, Matena A, Apostolakis K, Linne U, Zhukov I, Stanek J, Kozminski W, Davidson I, Secombes CJ *et al.* 2017. The RxLR motif of the host targeting effector AVR3a of *Phytophthora infestans* is cleaved before secretion. *Plant Cell* **29**: 1184–1195.

Whisson SC, Boevink PC, Moleleki L, Avrova AO, Morales JG, Gilroy EM, Armstrong MR, Grouffaud S, West PV, Chapman S *et al.* 2007. A translocation signal for delivery of oomycete effector proteins into host plant cells. *Nature* **450**: 115–118.

Whisson SC, Boevink PC, Wang S, Birch PR. 2016. The cell biology of late blight disease. *Current Opinion in Microbiology* **34**: 127–135.

Winn A, Ballard CC, Cowtan KD, Dodson EJ, Emsley P, Evans PR, Keegan RM, Krissinel EB, Leslie AGW, McCoy A *et al.* 2011. Overview of the CCP4 suite and current developments. *Acta Crystallographica. Section D, Biological Crystallography* **67**: 235–242.

Winter G. 2010. xia2: an expert system for macromolecular crystallography data reduction. *Journal of Applied Crystallography* **43**: 186–190.

Yang L, McLellan H, Naqvi S, He Q, Boevink PC, Armstrong M, Giuliani LM, Zhang W, Tian Z, Zhan J *et al.* 2016. Potato NPH2/RPT2-like protein StNRL1, targeted by a *Phytophthora infestans* effector, is a susceptibility factor. *Plant Physiology* **171**: 645–657.

Yin J, Gu B, Huang G, Tian Y, Quan J, Lindqvist-Kreuze H, Shan W. 2017. Conserved RXLR effector genes of *Phytophthora infestans* expressed at the early stage of potato infection are suppressive to host defence. *Frontiers in Plant Science* **8**: 2155.

Zhai Q, Yan L, Tan D, Chen R, Sun J, Gao L, Dong MQ, Wang Y, Li C. 2013. Phosphorylation-coupled proteolysis of the transcription factor MYC2 is important for jasmonate-signaled plant immunity. *PLoS Genetics* **9**: e1003422.

Zheng X, McLellan H, Fraiture M, Liu X, Boevink PC, Gilroy EM, Chen Y, Kandel K, Sessa G, Birch PRJ *et al.* 2014. Functionally redundant RXLR effectors from *Phytophthora infestans* act at different steps to suppress early flg22-triggered immunity. *PLoS Pathogens* **10**: e1004057.

Zheng X, Wagener N, McLellan H, Boevink PC, Hua C, Birch PRJ, Bruner F. 2018. *Phytophthora infestans* RXLR effector SFI5 requires association with calmodulin for PTI/MTI suppressing activity. *New Phytologist* **219**: 1433–1446.

Supporting Information

Additional supporting information may be found online in the Supporting Information section at the end of the article

Fig. S1 Representative leaf image showing *Phytophthora infestans* lesions following overexpression of each construct (GFP–PiSFI3, $_{NLS}$GFP–PiSFI3, or $_{NES}$GFP–PiSFI3) in *Nicotiana benthamiana*..

Fig. S2 PiSFI3 potato overexpression transgenic lines show enhanced *Phytophthora infestans* colonization.

Fig. S3 Transcript accumulation of flg22 maker genes posttreatment with flg22 on potato.

Fig. S4 SFI3 does not suppress programmed cell death triggered by INF1 or CF4/Avr4.

Fig. S5 Alignment of UBK/PUB33.

Fig. S6 PiSFI3 interacts with a potato protein containing U-box and kinase domains.

Fig. S7 Silencing *UBK* by VIGS in *Nicotiana benthamiana* or by RNAi in potato..

Fig. S8 Silencing *StUBK* by RNAi in potato enhance *Phytophthora infestans* colonization.

Fig. S9 VIGS of *UBK* does not compromise INF1 or Cf4/Avr4 cell deaths.

Fig. S10 Expression profile of *StUBK* posttreatment with flg22 and flg22 maker gene expression on *StUBK* RNAi lines post flg22 treatment.

Fig. S11 Overlays of the structures of the WY-domains of SFI3, Avr3a11 and PexRD2.

Fig. S12 SFI3 mutants lose nucleolar localisation.

Table S1 Primers used in this study.

Table S2 X-ray data collection and refinement statistics

Please note: Wiley Blackwell are not responsible for the content or functionality of any Supporting Information supplied by the authors. Any queries (other than missing material) should be directed to the *New Phytologist* Central Office.